CHAPTER

17

Biomedical Optics and Lasers

Gerard L. Coté, PhD, LiHong V. Wang, PhD, and Sohi Rastegar, PhD

OUTLINE

AT THE CONCLUSION OF THIS CHAPTER, STUDENTS WILL BE ABLE TO:

- Understand essential optical principles and fundamentals of light propagation in tissue, as well as other biological and biochemical media.
- Utilize basic engineering principles for developing therapeutic, diagnostic, sensing, and imaging devices with a focus on the use of lasers and optical technology.
- Describe the biochemical and biophysical interactions of optic and fiber optic systems with biological tissue.
- Understand the photothermal interactions of laser systems with biological tissue.

The use of light for therapeutic and diagnostic procedures in medicine has evolved from the use of sunlight for heat therapy and as a simple tool for the inspection of eyes, skin, and wounds to the current use of lasers and endoscopy in various medical procedures. The introduction of photonic technology into medicine over the last decade has revolutionized many clinical procedures and has the potential to continue to greatly impact health care. For example, coherent fiber optic bundles have been applied in laparoscopy cholecystectomy (minimally invasive removal of the gallbladder) to transform a once painful and expensive surgery into virtually an outpatient procedure. In the process, biomedical engineers have been instrumental in defining and demonstrating the engineering fundamentals of the interaction of light and heat with biological media, resulting in advances in dermatology, ophthalmology, cardiology, and urology.

Optical engineering has traditionally been taught as part of an electrical engineering curriculum and has been primarily applied in the development of defense and communications technologies. In biomedical optics applications, however, there are many issues related to the interaction of light with participating biological tissue/media that classical optics books and curricula do not cover. Therefore, the goal of this chapter is to provide students with a better understanding of the fundamental principles associated with the growing field of biomedical optics as well as advances in optically based therapeutic, diagnostic, and monitoring devices.

17.1 INTRODUCTION TO ESSENTIAL OPTICAL PRINCIPLES

Throughout the ages, great minds, including those of Galileo, Newton, Huygens, Fresnel, Maxwell, Planck, and Einstein, have studied the nature of light. Initially it was believed that light was either corpuscular or particle-like in nature or that it behaved as waves. After much debate and research, however, it has been concluded that there are circumstances where light behaves like waves and those where it behaves like particles. In this section, an overview of the behavior of light is described, beginning with the wave equation, which is commonly derived from Maxwell's equations. In addition, the optical spectrum and the fundamental governing equations for light absorption, scattering, and polarization are covered.

17.1.1 Electromagnetic Waves and the Optical Spectrum

It was in the late 1800s that J. Clerk Maxwell showed conclusively that light waves were electromagnetic in nature. This was accomplished by expressing the basic laws of electromagnetism and deriving from them the wave equation. The key to validating this derivation was that the free space solutions to the wave equation corresponded to electromagnetic waves with a velocity equal to the known experimental value of the velocity of light. Many introductory optics texts (such as the works of Hecht and Pedrotti) begin with the vectorial form for Maxwell's equations

$$\nabla^2 \mathbf{E} = \varepsilon_0 \mu_0 \, \partial^2 \mathbf{E} / \partial t^2 \tag{17.1}$$

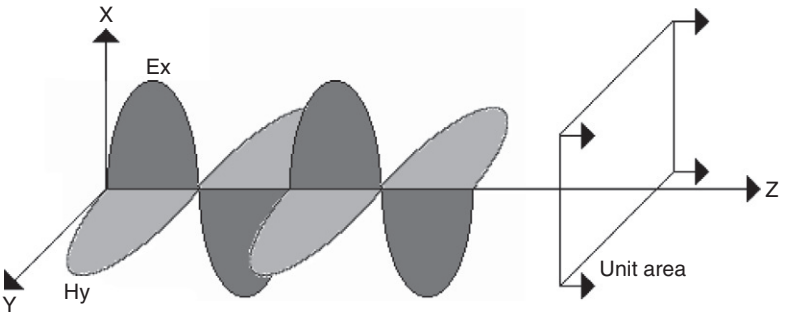

FIGURE 17.1 A sinusoidal electromagnetic wave.

where $\nabla^2\mathbf{E}$ is the partial second derivative of the electric field with respect to position ($\partial^2\mathbf{E}/dx^2 + \partial^2\mathbf{E}/dy^2 + \partial^2\mathbf{E}/dz^2$), ε is the electric permittivity of the medium, and μ is the magnetic permeability of the medium. In free space $\mu = \mu_0$ and $\varepsilon = \varepsilon_0$. From symmetry, there is a similar solution for the magnetic field (**H**). Since the wave velocity (c_0) is equal to the known value of the velocity of light, it can be expressed as follows:

$$c_0 = 1/(\varepsilon_0\,\mu_0)^{1/2} \tag{17.2}$$

Therefore, the change in the electric or magnetic field in space is related to the velocity and the change of the field with respect to time. Given Cartesian axes O_x, O_y, and O_z, shown in Figure 17.1, a typical solution to this wave equation is the sinusoidal solution given by

$$E_x = E_o \exp[j(\omega t - kz)] \tag{17.3}$$

$$H_y = H_o \exp[j(\omega t - kz)] \tag{17.4}$$

which states that the electric field oscillates sinusoidally in the X-Z plane, the magnetic field oscillates in the Y-Z plane (orthogonal to e-field and in phase), and the wave propagates in the O_z direction.

The frequency, f, and wavelength, λ, of the wave are related to the velocity, c, and given by

$$f = \omega/2\pi \tag{17.5}$$

$$\lambda = 2\pi/k \tag{17.6}$$

$$c = f\lambda = \omega/k \tag{17.7}$$

The ratio of the velocity of the wave in free space, c_o, to that in the medium through which the light propagates, c, is known as the index of refraction of the medium, $n = c_o/c$.

EXAMPLE PROBLEM 17.1

Given a red helium neon laser with a wavelength of 633 nm, determine the velocity of the light traveling through clear tissue, such as the cornea, that has an index of refraction of 1.33. How would this velocity change in glass that has an index of refraction of 1.5? Explain the significance of this result.

Continued

Solution

Rearranging the preceding equations,

$$c_{tissue} = c_0/n_{tissue} \simeq (2.998*10\text{^}8)/1.33 = 2.25*10\text{^}8 \text{ m/s for clear tissue}$$

while

$$c_{glass} = c_0/n_{glass} \simeq (2.998*10\text{^}8)/1.5 = 2.00*10\text{^}8 \text{ m/s for glass}$$

The significance of this result is that light travels faster through a material with a lower index of refraction, such as clear tissue (e.g., cornea, aqueous humor, and lens of the eye), compared to glass. This has many implications as you will see later in this chapter when it comes to determining the angle of reflection and refraction of light through differing materials and clear tissues.

The intensity or power per unit area of the wave can also be expressed in terms of the Poynting vector, **Π**—that is, defined in terms of the vector product of the electric and magnetic field as

$$\Pi = \mathbf{E} \times \mathbf{H} \tag{17.8}$$

The intensity of the wave is the average value of the Poynting vector over one period of the wave, so if E and H are spatially orthogonal and in phase, as shown in Figure 17.1, then

$$\mathbf{I} = \ < \Pi > \ = \text{power/unit area} = c\varepsilon\mathbf{E}^2 \tag{17.9}$$

where <**Π**> represents the average value of **Π**. For this equation it is clear that the intensity is proportional to the square of the electric field. This is true for the propagation of a wave through an isotropic dielectric medium. From Maxwell's equations it can be shown that the intensity is also proportional to the square of the magnetic field. Therefore, if the electric and magnetic fields were in phase quadrature (90 degrees out of phase), then the intensity would be zero, as shown following

$$\mathbf{I} =< \Pi >=< E_o \cos(\omega t)\, H_o \sin(\omega t) >= 0 \tag{17.10}$$

since the average value of a sine wave times a cosine wave is zero.

In addition to intensity, light can be characterized by its wavelength or, rather, electromagnetic spectrum, which ranges from low-frequency radio waves at 10^3 Hz to Gamma radiation at 10^{20} Hz. As depicted in Figure 17.2, the wavelength region of light can be divided into ultraviolet, which is 0.003 to 0.4 micrometers, to the visible region of 0.4 to 0.7 micrometers (7.5×10^{14} to 4.3×10^{14} Hz frequency range), to the near infrared region of 0.7 to 2.5 micrometers, to the mid-infrared region of 2.5 to 12 microns, and to the far infrared beyond 12 microns.

17.1.2 Optical Polarization

In the previous section the sinusoidal solution in terms of E_x and H_y is only one of an infinite number of such sinusoidal solutions to Maxwell's equations. The general solution for a sinusoid with angular frequency ω can be written as

$$\mathbf{E}(\mathbf{r}, t) = \mathbf{E}(\mathbf{r}) \exp(j\omega t) \tag{17.11}$$

in which **E**(**r**,t) and **E**(**r**) are complex vectors and **r** is a real radius vector.

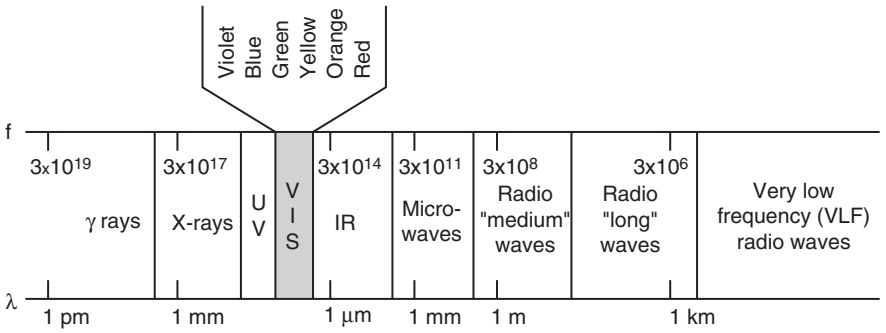

FIGURE 17.2 The electromagnetic spectrum.

For simplicity, consider the plane monochromatic (single wavelength) waves propagating in free space in the O_z direction; then the general solution to the wave equation for the electric field can be written as

$$E_x = e_x \cos(\omega t - kz + \delta_x) \tag{17.12}$$

$$E_y = e_y \cos(\omega t - kz + \delta_y) \tag{17.13}$$

in which δ_x and δ_y are arbitrary phase angles. This solution can be described completely by means of two waves (e-field in the X-Z plane and e-field in the Y-Z plane). If these waves are observed at a particular value of "z"—say, "z_o"—they take the oscillatory form

$$E_x = e_x \cos(\omega t + \delta'_x) \quad \delta'_x = \delta_x - kz_o \tag{17.14}$$

$$E_y = e_y \cos(\omega t + \delta'_y) \quad \delta'_y = \delta_y - kz_o \tag{17.15}$$

and the top of each vector appears to oscillate sinusoidally with time along a line. E_x is said to be linearly polarized in the direction O_x, and E_y is said to be linearly polarized in the direction O_y.

It can be seen from Eq. (17.15) that if the light is fully polarized, it can be completely characterized as a 2 by 1 matrix in terms of its amplitude and phase ($e_x \exp(j\delta'_x)$ and $e_y \exp(j\delta'_y)$). This vectoral representation is known as the Jones vector. When the optical system design includes the propagation of the light through nonscattering, and thus nondepolarizing, medium such as a lens or clear biological sample, the medium can be completely characterized by a 2 by 2 Jones matrix. Therefore, the output of the propagation of the polarized light can be modeled as a multiplication of the Jones matrix of the optical system and the input light vector. A system that yields both polarized and partially polarized light, such as that obtained from tissue scattering, can be characterized using 4 by 4 matrices known as Mueller matrices and a 4 by 1 matrix known as the Stokes vector.

Returning back to Eq. (17.15), the tip of the polarized light vector is the vector sum of E_x and E_y which, in general, is an ellipse as depicted in Figure 17.3 whose Cartesian equation in the X-Y plane at $z = z_o$ is

$$E_x^2/c_x^2 + E_y^2/c_y^2 + 2(E_xE_y/e_xe_y)\cos\delta = \sin^2\delta \tag{17.16}$$

in which $\delta = \delta_y' - \delta_x'$. It should be noted that the ellipse folds into a straight line, producing linear light if (1) $E_x \neq 0$ and $E_y = 0$, or (2) $E_y \neq 0$ and $E_x = 0$, or (3) $\delta = m\pi$ in which m is a positive or negative integer. The light becomes circular if $e_x = e_y$ and $\delta = (2m + 1)\pi/2$, since E_x and E_y would then have equal amplitudes and be in phase quadrature.

The polarization properties of light become particularly important for anisotropic media in which the physical properties are dependent on direction (i.e., E_x is different from E_y and thus values e_x, e_y, and δ will vary along the propagation path, as depicted with a birefringent crystal, polarization preserving optical fiber, or aligned tissue fibers such as collagen).

EXAMPLE PROBLEM 17.2

Consider a general solution to the wave equation represented as a plane electromagnetic wave (in SI units) given by the expressions

$$E_x = 0, \qquad E_z = 0, \qquad E_y = 2\cos[2\pi * 10^{14}\,(t - x/c) + \pi/2]$$

For the equations shown, determine the frequency (f), wavelength (λ), direction of motion (x, y, or z), amplitude (A), initial phase angle (ϕ), and polarization of the wave (linear, circular, elliptical).

Solution

The general form of a plane electromagnetic wave can be expressed as $E = A\cos(kx \pm \omega t + \phi)$, where $k = 2\pi/\lambda$, $\lambda = c/f$, $\omega = 2\pi f$, and $c = 3*10^8$ meters/second. The preceding equation can therefore be written in general form as $E_y = 2\cos[2\pi*10^{14}\,t - (2\pi*10^{14}\,x/c) + \pi/2]$. Thus, comparing the two equations yields the values $f = 1*10^{14}$ Hertz, $\lambda = 3*10^{-6} = 3$ micrometers, motion is in the positive x direction, A = 2 Volts/meter, $\phi = \pi/2$, and since $E_x = E_z = 0$, the wave must be linearly polarized in the *y* direction.

17.1.3 Absorption, Scattering, and Luminescence

Having discussed polarization, attention will now be focused on the optical properties of light that describe the changes in the light as it passes through biological media. The optical properties of the light are defined in terms of the absorption, scattering, and anisotropy of

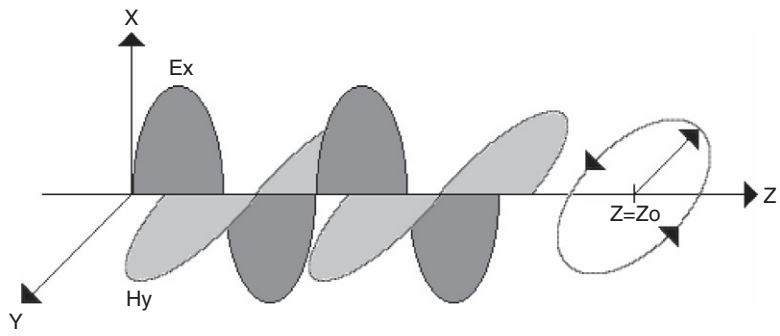

FIGURE 17.3 Polarization propagation of an **E** wave.

the light. Knowing the absorption, scattering, and direction of propagation of the light has applications for both optical diagnostics and sensing, as well as optical therapeutics. For instance, many investigators are trying to quantifiably and noninvasively measure certain body chemicals such as glucose using the absorption of light. In addition, by knowing the absorption and scattering of light, investigators are modeling the amount of coagulation or "cooking" of the tissue that is expected for a given wavelength of light, such as in the case of prostate surgery or cancer therapy.

The optical penetration depth and the volume of tissue affected by light is a function of both the light absorption and scattering. If it is assumed scattering is negligible or, rather, absorption is the dominant component, then the change in light intensity is determined by the absorption properties in the optical path and the illumination wavelength. For instance, for wavelengths above 1.5 micrometers, the light propagation through all biological tissues, since they have large water content, is absorption dominant. The intensity relationship as a function of optical path and concentration for this absorption dominant case can be described by the Beer-Lambert law as

$$I(z) = I_o \exp(-\mu_a z) \tag{17.17}$$

in which I is the transmitted light intensity, I_o is the incident light intensity, z is the path length of the light, and μ_a (1/cm) is the absorption coefficient. The absorption coefficient can be further broken down into two terms that include the concentration of the chemically absorbing species, C (mg/mL), times the molar absorptivity, v (cm^2/mg), which is a function of wavelength.

Luminescence, also known as fluorescence or phosphorescence, depending on the fluorescent lifetime, is a process that occurs when photons of electromagnetic radiation are absorbed by molecules, raising them to some excited state, and then, on returning to a lower energy state, the molecules emit radiation or rather luminesce. Fluorescence does not involve a change in the electron spin and therefore occurs much faster. The energy absorbed in the luminescence process can be described in discrete photons by the equation

$$E = hc/\lambda \tag{17.18}$$

in which E is the energy, h is Planck's constant (6.626×10^{-34} J-s), c is the speed of light, and λ is the wavelength. This absorption and reemission process is not 100 percent efficient, since some of the originally absorbed energy is dissipated before photon emission. Therefore, the excitation energy is greater than that emitted

$$E_{\text{excited}} > E_{\text{emitted}} \tag{17.19}$$

and

$$\lambda_{\text{emitted}} > \lambda_{\text{excited}} \tag{17.20}$$

The energy level emitted by any fluorochrome is achieved as the molecule emits a photon, and because of the discrete energy level, individual fluorochromes excited by a given wavelength typically only fluoresce at a certain emission wavelength. Originally fluorescence was used as an extremely sensitive, relatively low-cost technique for sensing dilute solutions. Only recently have investigators used fluorescence in turbid media such as tissue for diagnostics and sensing.

It is well known that tissues scatter as well as absorb light, particularly in the visible and near-infrared wavelength regions. Scattering, unlike absorption and luminescence, need not involve a transition in energy between quantized energy levels in atoms or molecules but rather is typically a result of random spatial variations in the dielectric constant. Therefore, the actual light distributions can be substantially different from distributions estimated using Beer's law. In fact, light scattered from a collimated beam undergoes multiple scattering events as it propagates through tissue. The transport equation that describes the transfer of energy through a turbid medium (a medium that absorbs and scatters light) is an approach that has been proven to be effective. The transport theory has been used to describe scattering, absorption, and fluorescence, but until recently, polarization has not been included, in part because it takes relatively few scattering events to completely randomize the polarization of the light beam. The transport theory approach is discussed later in this chapter and is a heuristic theory based on a statistical approximation of photon particle transport in a multiple scattering medium.

17.2 FUNDAMENTALS OF LIGHT PROPAGATION IN BIOLOGICAL TISSUE

In this section the propagation of light through biological media such as tissue is discussed, beginning with a simple ray optics approach for light traveling through a nonparticipating media, where the effect of the absorption and scatter within the media is ignored. The effects of absorption and scatter on light propagation are then discussed, along with the consideration of boundary conditions and various means of measuring the optical absorption and scattering properties.

17.2.1 Light Interactions with Nonparticipating Media

Previously we defined *light* as a set of electromagnetic waves traveling in the O_z direction. In this section light is treated as a set of "rays" traveling in straight lines that, when combined, make up the plane waves described using the preceding complex exponentials. This approach is important in order to study the effect on the light at the boundaries between two different optical media. In the treatment of geometrical or ray optics of the light, it is first assumed that the incident, reflected, and refracted rays all lie in the same plane of incidence. The propagation at the boundary between these two interfaces, as shown in Figure 17.4, is based on two basic laws—namely, the angle of reflection equals the angle of incidence, and the sine of the angle of refraction bears a constant ratio to the sine of the angle of incidence (Snell's law). It should be noted that ray propagation can be very useful for a good majority of the applications considered with the propagation of the light through bulk optics such as in the design of lenses and prisms. It has severe limitations, however, in that it cannot be used to predict the intensities of the refracted and reflected rays, nor does it incorporate the effects of scatter and absorption. In addition, when apertures are used that are smaller than the bulk combined rays, a wave process known as diffraction occurs that causes the geometrical theory to break down and the beams to diverge.

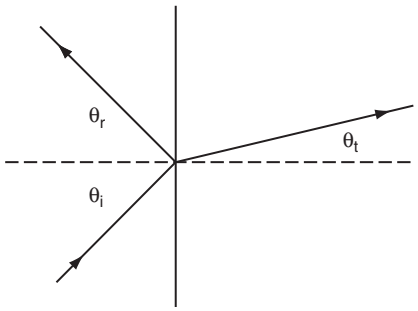

FIGURE 17.4 Ray propagation of light at the boundary of two interfaces. Clearly the angle of incidence equals the angle of reflection ($\theta_i = \theta_r$) and from Snell's law the sine of the angle of refraction bears a constant ratio to the sine of the angle of incidence ($n_i \sin(\theta_i) = n_t \sin(\theta_t)$).

EXAMPLE PROBLEM 17.3

A green light beam hits the cornea of the eye, making an angle of 25 degrees with the normal, as depicted following.

(a) Determine the output angle from the front surface of the cornea and into the cornea, given that the index of refraction of air is 1.000, and that of the cornea is 1.376.

(b) What can be said about how the cornea bends the light?

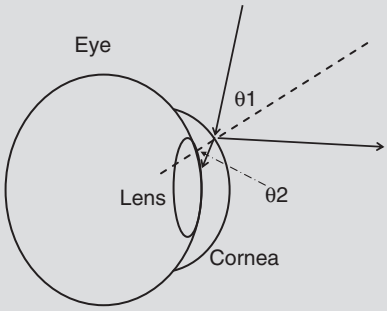

Solution

(a) Snell's law, n1 sin(θ1) = n2 sin(θ2), can be rearranged to calculate θ2 in the lens.

$$\theta 2 = \sin^{-1}(1.000 \sin(25)/1.376) = 17.89 \text{ degrees}$$

(b) It has been shown and can be said that the cornea tends to bend the light toward the normal as it passes through. This makes sense because the eye is made to bend the light so it can pass through the center iris and lens toward the retina to be imaged by the brain.

Wave theory is used to describe the phenomena of reflection and refraction in an effort to determine the intensity of the light as it propagates from one medium to another. If two nonconducting media are considered, as in Figure 17.4, the boundary conditions follow from Maxwell's equations such that the tangential components of **E** and **H** are continuous across the boundary $\mathbf{E}_i + \mathbf{E}_p = \mathbf{E}_t$, and the normal components of

B (the magnetic flux density) and **D** (the electric displacement) are continuous across the boundary. These conditions can only be true at all times and all places on the boundary if the frequencies of all waves are the same. The relative amplitudes of the waves will now be considered (note the values of **E**, **H**, **D**, and **B** will depend on the direction of vibration of **E** and **H** fields of the incident wave relative to the planes of incidence). In other words, they depend on the polarization of the wave. The wave can be divided into two orthogonal polarization states, and using Maxwell's equations, Snell's law, and the law of reflection as well as imposing the boundary conditions, the following Fresnel equations can be derived. The reflected and transmitted equations in the parallel configuration are

$$r_{\mathrm{p}} = \left(\frac{E_r}{E_i}\right)_{\mathrm{p}} = (-n_i \cos\theta_{\mathrm{t}} + n_t \cos\theta_{\mathrm{i}})/(n_i \cos\theta_{\mathrm{t}} + n_t \cos\theta_{\mathrm{i}}) \tag{17.21}$$

$$t_{\mathrm{p}} = \left(\frac{E_t}{E_i}\right)_{\mathrm{p}} = (2n_i \cos\theta_{\mathrm{i}})/(n_i \cos\theta_{\mathrm{t}} + n_t \cos\theta_{\mathrm{i}}) \tag{17.22}$$

The normal or perpendicular reflected and transmitted equations are

$$r_{\perp} = \left(\frac{E_r}{E_i}\right)_{\perp} = (n_i \cos\theta_{\mathrm{i}} - n_t \cos\theta_{\mathrm{t}})/(n_i \cos\theta_{\mathrm{i}} + n_t \cos\theta_{\mathrm{t}}) \tag{17.23}$$

$$t_{\perp} = \left(\frac{E_t}{E_i}\right)_{\perp} = (2n_i \cos\theta_{\mathrm{i}})/(n_i \cos\theta_{\mathrm{i}} + n_t \cos\theta_{\mathrm{t}}) \tag{17.24}$$

Using the preceding equations, there are two noteworthy limiting cases. The first case is as follows. If $n_t > n_i$, then $\theta_{\mathrm{i}} > \theta_{\mathrm{t}}$, $r_{\perp}$ is always negative for all values of θ_{i}, and r_{p} starts out positive at $\theta_{\mathrm{i}} = 0$ and decreases until it equals 0 when $\theta_{\mathrm{i}} + \theta_{\mathrm{t}} = 90^{\mathrm{o}}$. This implies that the refracted and reflected rays are normal to each other, and from Snell's law this occurs when $\tan\theta_{\mathrm{i}} = n_t/n_i$. This particular value of θ_{i} is known as the polarization angle or, more commonly, the Brewster angle. At this angle only the polarization with **E** normal to the plane of incidence is reflected, and as a result, this is a useful way of polarizing a wave. Now, as θ_{i} increases beyond θ_{p}, r_{p} becomes progressively negative, reaching –1.0 at 90^{o}, which implies that the surface performs as a perfect mirror at this angle. On the other hand, at normal incidence $\theta_{\mathrm{i}} = \theta_{\mathrm{r}} = \theta_{\mathrm{t}} = 0$, then $t_{\mathrm{p}} = t_{\perp} = 2n_i/(n_i + n_t)$ and $r_{\mathrm{p}} = -r_{\perp} = (n_t - n_i)/(n_i + n_t) = -(n_i - n_t)/(n_i + n_t)$. The wave intensity, which is what can actually be measured by a detector, is defined proportional to the square of the electric field. Thus, $(I_{\mathrm{R}}/I_i) = (r_{\mathrm{p}})^2 = \left(\frac{E_r}{E_i}\right)^2 = (n_t - n_i)^2/(n_i - n_t)^2$ and $(I_t/I_i) = (t_{\mathrm{p}})^2 = \left(\frac{E_t}{E_i}\right)^2 = 4n_i^2/(n_i + n_t)^2$. The preceding expressions are useful because they represent the amount of light lost by normal specular reflection when transmitting from one medium to another.

The second limiting case is, if $n_t < n_i$, then $\theta_{\mathrm{t}} > \theta_{\mathrm{i}}$, $r_{\perp}$ is always positive for values of θ_{i}, and $r_{\perp}$ increases from its initial value at $\theta_{\mathrm{i}} = 0$ until it reaches +1.0 at what is known as the critical angle θ_{c}. At this angle $\theta_{\mathrm{i}} = \theta_{\mathrm{c}}$, then $\theta_{\mathrm{t}} = 90^{\mathrm{o}}$, and from Snell's law, $\sin\theta_{\mathrm{t}} = n_i/n_t \sin\theta_{\mathrm{i}}$. Clearly for $n_i > n_t$ (less dense to more dense medium), $\sin\theta_{\mathrm{t}}$ could be greater than one, according to the preceding equation. This is not possible for any real value of θ_{t},

and thus the angle for which $\theta_i = \theta_c$ is when $(n_i/n_t) \sin \theta_c = 1$ or, rather, $\theta_t = 90^o$. Thus, for all values of $\theta_i > \theta_c$, the light is totally reflected at the boundary. This phenomenon is what is used for the creation of optical fibers, in which the core of the fiber (where the light is supposed to propagate) has an index of refraction slightly higher than the cladding surrounding it, so the light launched into the fiber will totally internally reflect allowing for minimally attenuated propagation down the fiber.

17.2.2 Light Interaction with Participating Media: The Role of Absorption and Scattering

When light is incident on tissue either from a laser or from other light transmitting devices, tissue acts as a participating medium by reflecting, absorbing, scattering, and transmitting various portions of the incident wave of radiation. Ideally, an electromagnetic analysis of the light distribution in the tissue would be performed. Unfortunately, this can be quite cumbersome, and a reliable database of electrical properties of biological tissues would be required. An alternate practical approach to the problem is to use transport theory that starts with the construction of the differential equation for propagation of the light intensity. In the following section, the equation for light intensity distribution in a purely absorbing medium will be derived. With this motivation, the next section introduces the general equation of transfer for a medium that scatters as well as absorbs the light.

The Case of Pure Absorption

In order to describe the distribution and transport of laser energy in a nontransparent participating medium, the medium can be viewed as having two coexisting "phases": a material phase for all the masses of the system and a photon phase for the electromagnetic radiation. Figure 17.5 shows the material phase as circles and the photon phase as curved arrows that strike the material phase. The energy balance equation for the material phase is introduced and discussed in the thermodynamic descriptions in Sections 17.3 and 17.5. The energy balance equation for the photon phase is discussed following.

Consider an infinitesimal volume of the material under irradiation (Figure 17.6). The rate of change of radiative energy, $U^{(rad)}$, with time is the difference between the incoming and outgoing radiative fluxes in the element minus the rate of energy absorption by the material phase. The difference between the incoming and outgoing fluxes is, in the limit, the negative of the divergence of the radiative flux. Therefore, denoting the energy absorbed by the material phase, which is the laser heat source term, by Q_L and the radiative flux by $\vec{q}^{(rad)}$ the governing differential equation for energy rate balance in the photon phase can be written as

$$\partial U^{(rad)} / \partial t = -\vec{\nabla} \cdot \vec{q}^{(rad)} - Q_L \tag{17.25}$$

Any possible photon emission or scattering by the material phase has been ignored.

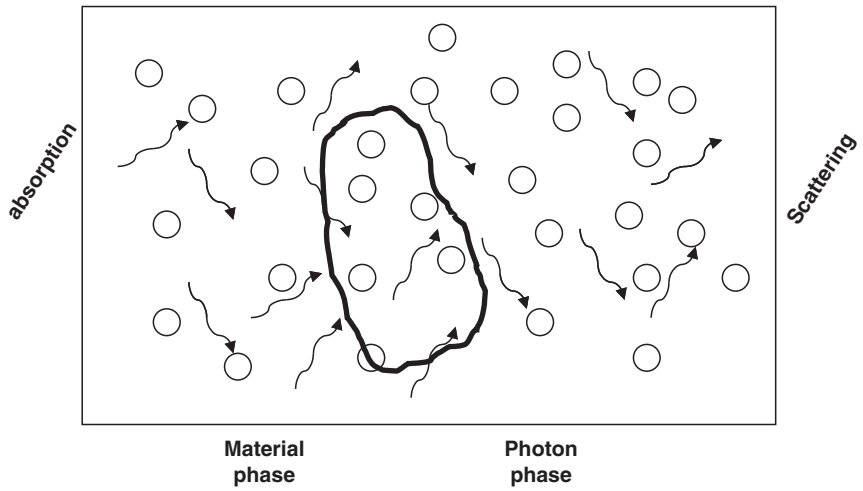

FIGURE 17.5 Two coexisting phases, the photon phase (laser) and the material phase (tissue) govern laser-tissue interactions. Photons are distributed within the tissue by the processes of absorption and scattering. Energy balance over a control volume (shown with thicker line) provides the governing equation for light and heat distribution and exchange of energy between the photon and material phase as described later in the chapter.

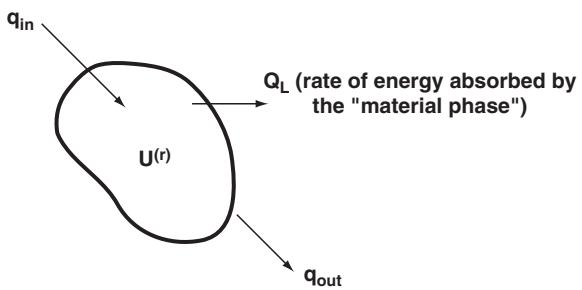

FIGURE 17.6 Control volume of the photon phase with radiative fluxes in and out, radiative energy, and rate of energy lost to the material phase by absorption.

For a steady-state system in which radiation is collimated and monochromatic, laser light travels only in the positive z direction—that is, assuming only one forward flux—Eq. (17.25) reduces to

$$dq_z^{(rad)}/dz = -Q_L. \tag{17.26}$$

Considering the speed of light and the dimensions of a biological tissue, the assumption of a steady-state condition is a reasonable assumption for most applications except when very fast light sources are used and/or when time-resolved analyses are considered. The important step at this point is to use the phenomenological relation

$$Q_L = \mu_a I \tag{17.27}$$

where μ_a is defined as the absorption coefficient and I is the total light intensity. The total intensity at a point is the sum of radiative fluxes received at that point. In the case presented here, using purely absorbing tissue, a single radiative flux is used, and thus,

$$I = q_z^{(rad)} \tag{17.28}$$

Proceeding by replacing Eqs. (17.27) and (17.28) into Eq. (17.26), the following differential equation is obtained

$$\frac{dI}{dz} = -\mu_a I \tag{17.29}$$

which has the simple solution

$$I(z) = I_0 \exp(-\mu_a z) \tag{17.30}$$

where I_0 denotes the intensity at the surface, $z = 0$. This equation is the well-known *Beer-Lambert* law of absorption, as given in Eq. (17.17) for a purely absorbing medium, which was mentioned earlier in the chapter.

The laser heat source term can now be written (Eqs. (17.27) and (17.30)) as

$$Q_L = \mu_a I_0 \exp(-\mu_a z). \tag{17.31}$$

This equation can be generalized to an axisymmetric three-dimensional case to include the effect of the radial beam profile of a laser light incident orthogonally on a slab by writing it as

$$Q_L(r, z) = \mu_a I_0 \exp(-\mu_a z) f(r), \tag{17.32}$$

where $f(r)$ is the radial profile of an axisymmetric laser beam. For a Gaussian beam profile, which is a common mode of laser irradiation,

$$f(r) = \exp\left(-\frac{2r^2}{\omega_o^2}\right) \tag{17.33}$$

where ω_o is known as the "$1/e^2$ radius" of the beam, since at $r = \omega_o$, $f(r) = 1/e^2$.

EXAMPLE PROBLEM 17.4

For a Gaussian laser beam irradiating at a wavelength of 2.1 μm, the absorption coefficient is estimated to be 25 cm^{-1} and scattering is negligible. The radial profile of light intensity and the rate of heat generation at the tissue surface, $z = 0$, and its axial profile along the center axis of the beam, $r = 0$, can be found using Eqs. (17.32) and (17.33). Graph $I(r, 0)$ for r ranging from $-2\omega_o$ to $+ 2\omega_o$ and $I(0, z)$ for $z = 0$ to $z = 5/\mu_a$, as well as graph $Q_L(r, 0)$ and $Q_L(0, z)$. For simplicity, $I_o = 1$ W/cm^2 can be used.

Solution

Plot of the radial and axial profile of light intensity, I, and volumetric rate of absorption, Q_L, in a purely absorbing tissue.

Continued

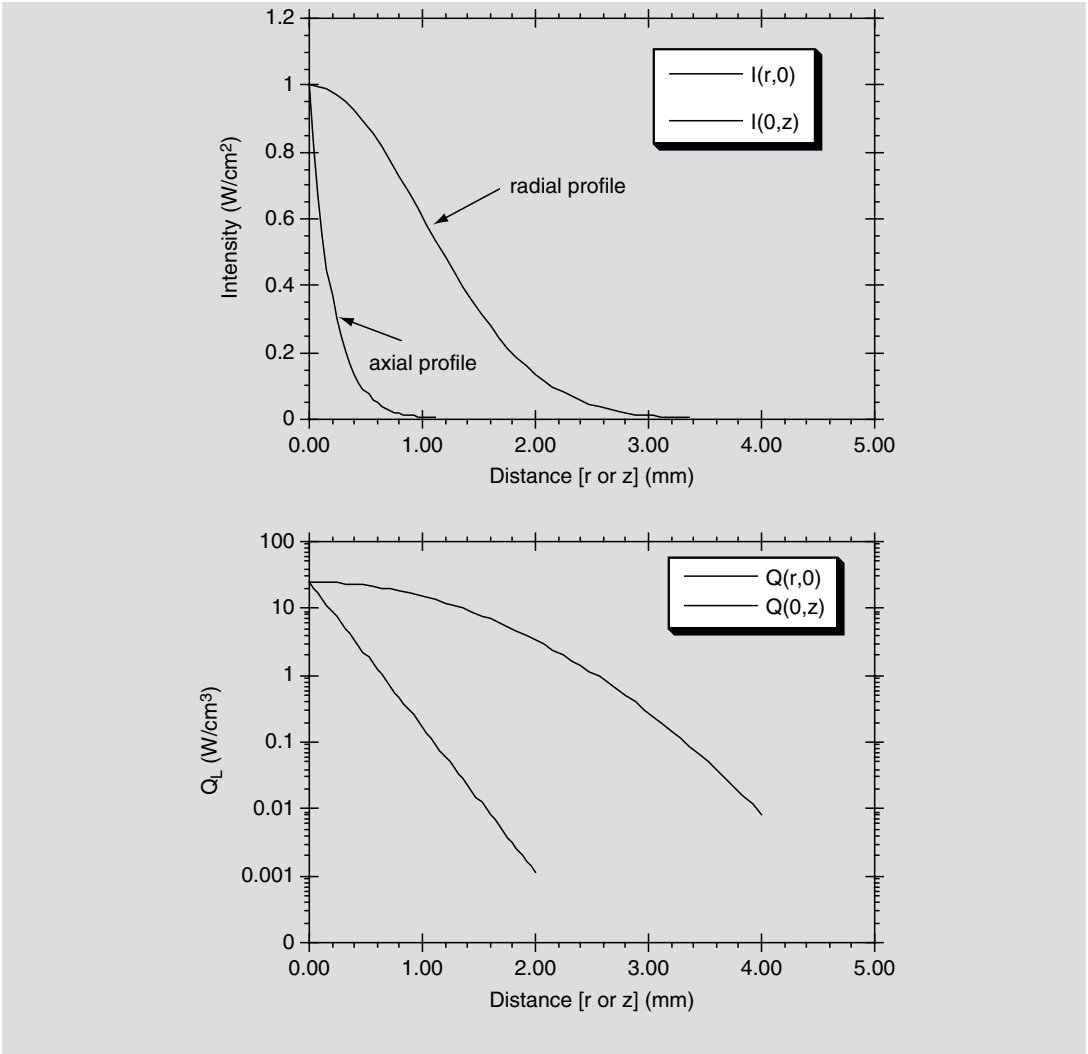

Methods for Scattering and Absorbing Media

The fundamental quantity in the transport theory approach is the total specific intensity, L, which is a function of position $\vec{r}$ for light in the direction given by a unit vector $\hat{s}$ and its units are $W\ .cm^{-2}\ .s^{-1}$. The equation of transfer satisfied by L can be written as

$$\frac{dL(\vec{\mathrm{r}},\hat{\mathrm{s}})}{ds} = -(\mu_{\mathrm{a}}+\mu_{\mathrm{s}})L(\vec{\mathrm{r}},\hat{\mathrm{s}}) + \mu_{\mathrm{s}}\int_{4\pi} p(\hat{\mathrm{s}},\hat{\mathrm{s}}')L(\vec{\mathrm{r}},\hat{\mathrm{s}}')d\omega' + \mathrm{S}(\vec{\mathrm{r}},\hat{\mathrm{s}}) \tag{17.34}$$

Equation (17.34) shows the decrease in L due to scattering μ_s and absorption μ_a and the increase in L due to scattering from L coming from another direction $\hat{s}'$ (Figure 17.7). The sum

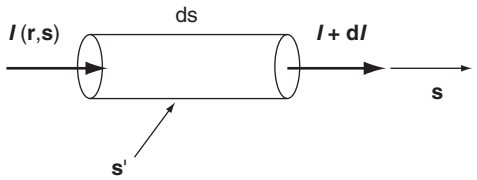

FIGURE 17.7 Light intensity change in the transport theory approach including scattered light from other directions.

of scattering and absorption, $\mu_t = \mu_a + \mu_s$, is defined as the attenuation coefficient. The function $p(\hat{s}, \hat{s}')$ is called the "phase function" and is related to the scattering amplitude of a particle, a scaled form of the probability distribution of scattering angles. Note that by ignoring scattering and assuming a collimated light source, Eq. (17.34) reduces to Eq. (17.29), which was derived in the last subsection. $S(\vec{r}, \hat{s})$ is the source term that could be irradiation on the surface, fluorescence generated inside the tissue, or an internal volumetric light source.

The equation of transfer is an integro-differential equation for which a general solution does not exist. However, several approximate solutions have been found, such as the two-flux and multiflux models, the discrete ordinate finite element method, the spherical harmonic method, the diffusion approximation, and the Monte Carlo method. Each of these is subject to certain limitations and assumptions. In this chapter the focus is on the diffusion approximation, which is one solution.

Diffusion Approximation

The diffusion approximation is a second-order differential equation that can be derived from the radiative transfer equation (17.34) under the assumption that the scattering is "large" compared with absorption. The solution to this equation provides a useful and powerful tool for the analysis of light distribution in turbid media. The governing differential equation for the diffusion approximation is

$$\nabla^2 \phi_d - 3\mu_a \mu_t' \phi_d = -\frac{\mu_s'}{D}\phi_c \tag{17.35}$$

where ϕ_d is the diffuse fluence rate and the parameters of the equation are $\mu_s' = \mu_s(1 - g)$, $\mu_t' = \mu_a + \mu_s'$ and $D = 1/3\ \mu_t'$, in which g is defined as the anisotropy of the medium.

The total light fluence rate, ϕ [W/cm^2], is the sum of the collimated part, ϕ_c, and the diffuse part, ϕ_d. The total fluence rate, as given by the following equation, is a key parameter in laser-tissue interaction. It can be thought of as the total light received at a point in space, or within the medium, through a small sphere divided by the area of that sphere.

$$\phi(r, z) = \phi_c(r, z) + \phi_d(r, z). \tag{17.36}$$

The collimated fluence rate is given by

$$\phi_c = I_o(r)\ (1 - r_{sp})\ \exp(-\mu_t' z), \tag{17.37}$$

where I_o is the surface flux density [W/cm^2] of the incident beam and r_{sp} is the specular reflectance. The optical boundary condition at the beam axis ($r = 0$) is

$$\left.\frac{\partial \phi_d}{\partial r}\right|_{r=0} = 0. \tag{17.38}$$

The boundary condition elsewhere is

$$\phi_d - 2AD\,\nabla\phi_d \bullet \tilde{n} = 0 \tag{17.39}$$

where A is the internal reflectance factor and $\tilde{n}$ is the inward unit normal vector. The internal reflectance factor A can account for the effect of mismatch in the index of refraction between the boundary and the surrounding medium and is given by

$$A = \frac{1 + r_i}{1 - r_i} \tag{17.40}$$

where r_i is evaluated by an empirical formula

$$r_i = -1.440\, n_{\text{rel}}^{-2} + 0.710\, n_{\text{rel}}^{-1} + 0.688 + 0.0636\, n_{\text{rel}}, \tag{17.41}$$

and n_{rel} is the ratio of the refractive indices of the tissue and the medium. The internal reflectance factor A reduces to 1 in cases where the boundary is matched—that is, when $n_{\text{rel}} = 1$.

Equations (17.35) through (17.41) provide the governing differential equations and boundary condition for the diffusion approximation. A solution of these, either by analytical or numerical methods, allows the calculation and analysis of fluence rates within a scattering and absorbing media such as biological tissues. As an example, for an isotropic point source inside an infinite medium, the solution for fluence rate as measured by a detector embedded inside the medium at a "large" distance r from the fiber can be derived using the Green's functions solution of the preceding equations to be

$$\phi(r) = \frac{\phi_o}{4\pi D}\,\frac{e^{-r/\delta}}{r} \tag{17.42}$$

where δ ($= \sqrt{D/\mu_a}$) is the penetration depth.

EXAMPLE PROBLEM 17.5

It is desired to measure the concentration of an absorber in a scattering medium with known scattering coefficient. If the reduced scattering coefficient μ_s' is known and the relative intensity at a distance r_o from an isotropic source can be measured, solve an algebraic equation for the absorption coefficient based on the diffusion approximation given r_o is large enough for diffusion approximation to be valid.

Solution

Given scattering coefficients μ_s', r_o, and $\phi(r_o)/\phi_o$, an algebraic equation for μ_a based on the diffusion approximation is required.

$$\begin{aligned} \phi(\mathrm{r}) &= \phi_o \exp(-\mathrm{r}/\delta)/(4\,\pi\,\mathrm{D}\,\mathrm{r}) \\ \log[\phi(\mathrm{r})/\phi_\mathrm{o}] &= -\mathrm{r}/\delta - [\log 4 + \log \pi + \log \mathrm{D} + \log \mathrm{r}] \\ \mathrm{D} &= 1/3\mu_{t'} \\ \delta &= \sqrt{\mathrm{D}/\mu_\mathrm{a}} \end{aligned} \tag{ex.1}$$

The left-hand side of Eq. (ex.1) is a known value—say, k_1:

$$\begin{aligned} \therefore \mathrm{k}_1 &= -\mathrm{r}/\delta - [\log 4 + \log \pi + \log \mathrm{D} + \log \mathrm{r}] \\ \therefore \mathrm{k}_1 + \log 4 + \log \pi + \log \mathrm{r} &= -\mathrm{r}/\delta - \log \mathrm{D} \end{aligned} \tag{ex.2}$$

The left-hand side of Eq. (ex.2) is again a known value—say, k_2:

$$\begin{aligned} \therefore \mathrm{k}_2 &= -\mathrm{r}/(\sqrt{\mathrm{D}/\mu_a}) - \log \mathrm{D} \\ \therefore \mathrm{k}_2 &= -\mathrm{r}\,(\sqrt{\mu_a/\mathrm{D}}) - \log \mathrm{D} \\ \therefore \mathrm{k}_2 &= -\mathrm{r}\,(\sqrt{\mu_a/1}/(3\mu_t')) - \log(1/3\mu_t') \\ \therefore \mathrm{k}_2 &= -\mathrm{r}\,(\sqrt{3\mu_a\mu_t'}) - \log\,(1/3\mu_t') \\ \therefore \mathrm{k}_2 &= -\mathrm{r}\,(\sqrt{3\mu_a(\mu_a+\mu_s')}) - \log\,(1/3(\mu_a+\mu_s')) \end{aligned} \tag{ex.3}$$

Solving Eq. (ex.3), the value of the coefficient of absorption can be found.

17.2.3 Measurement of Optical Properties

The measurement of optical properties—namely, absorption coefficient (μ_a), scattering coefficient (μ_s), and scattering anisotropy (g)—of biological tissues is an important problem in the field of biomedical optics. Knowledge of these parameters is important in both therapeutic and diagnostic applications of light in medicine. For example, optical properties are required to predict fluence distributions for irradiation procedures such as photodynamic therapy, photocoagulation, and tissue ablation. Also, in addition to having a profound impact on in vivo diagnostics such as fluorescence spectroscopy and optical imaging, the optical properties themselves can potentially be used to provide metabolic information and diagnose diseases.

To date, a number of methods have been developed to measure tissue optical properties. The collimated transmission technique can be used to measure the total interaction coefficient ($\mu_a + \mu_s$). In this technique, a collimated light beam illuminates a thin piece of tissue. Unscattered transmitted light is detected, while the scattered light is rejected by use of a small aperture. The unscattered transmitted light can be calculated based on the Beer-Lambert law, which is an extension of Eq. (17.30). The Beer-Lambert law for absorbing and scattering media is $I(z) = \mathrm{I}_0 \exp[-(\mu_a + \mu_s)\, z]$, where $I(z)$ is the unscattered transmitted light intensity after penetrating a depth of z. In collimated transmission measurements, I_0, $I(z)$, and z are measured. Therefore, $\mu_a + \mu_s$ can be deduced.

EXAMPLE PROBLEM 17.6

A 5 mW collimated laser beam passes through a 4 cm nonabsorbing, scattering medium. The collimated transmission was measured through a small aperture to be 0.035 mW. Calculate the scattering coefficient.

Solution

Based on Beer's law, $\mu_s = \ln(5/0.035)/4 = 1.2\ \text{cm}^{-1}$.

One of the earliest techniques developed for experimentally measuring absorption and scatter is the integrating sphere measurement method. In this technique, a thin slice of tissue is sandwiched between two integrating spheres (spheres with an entrance and exit port whose inner surface is coated with a diffuse reflecting material). A collimated beam is incident upon the tissue sample. Both the diffuse reflectance and transmittance are measured by integrating the diffusely reflected and transmitted light, respectively. These two measurements are used to deduce the absorption coefficient (μ_a) and the reduced scattering coefficient (μ_s') with a model. The model could be based on the adding-doubling method, the delta-Eddington method, the Monte Carlo method, or other light transport theories.

Another technique is normal incidence video reflectometry. A collimated light beam is normally incident upon a tissue. The spatial distribution of diffuse reflectance is collected using either a CCD camera or an optical fiber bundle. Diffusion theory is used to fit the measured spatial distribution of diffuse reflectance to determine the optical properties. The measured spatial distribution of diffuse reflectance must be in absolute units unless total diffuse reflectance is measured along with the diffuse reflectance profile. Calibration to absolute units is a sensitive procedure, so this method is not ideal for a clinical setting.

It is possible to use time-resolved or frequency-domain techniques to measure optical properties. But these techniques require instrumentation that may not be cost effective for nonresearch applications. One promising approach for in vivo optical property measurements is fiber optic–based oblique incidence reflectometry. It is a fairly accurate method for measuring the absorption and reduced scattering coefficients, μ_a and μ_s', providing the sample can be regarded as a semi-infinite turbid media, as is the case for most in vivo tissues. Therefore, this approach will be covered in more detail in this section.

Obliquely incident light produces a spatial distribution of diffuse reflectance that is not centered about the point of light incidence. The amount of shift in the center of diffuse reflectance is directly related to the medium's diffusion length, D. A fiber optic probe may be used to deliver light obliquely and sample the relative profile of diffuse reflectance. Measurement in absolute units is not necessary. From the profile, it is possible to measure D, perform a curve fit for the effective attenuation coefficient, μ_{eff}, and then calculate μ_a and μ_s'. Here, μ_{eff} is defined as

$$\mu_{eff} = \sqrt{\mu_a / D} \tag{17.43}$$

The spatial distribution of diffuse reflectance of normally incident light has previously been modeled using two isotropic point sources, one positive source located 1 transport

mean free path (mfp′) below the tissue surface and one negative image source above the tissue surface. The positive source represents a single scatter source in the tissue, and the height in z of the image source depends on the boundary condition. The transport mean free path is defined as

$$mfp' = 1/(\mu_a + \mu_s') \tag{17.44}$$

With oblique incidence, the buried source should be located at the same path length into the tissue, with this distance now measured along the new optical path as determined by Snell's law. It is assumed that (a) the angle of incidence and (b) the indexes of refraction for both the tissue and the medium through which the light is delivered are known. The net result is a change in the positions of the point sources, particularly a shift in the x direction. These two cases are shown in Figures 17.8a and b.

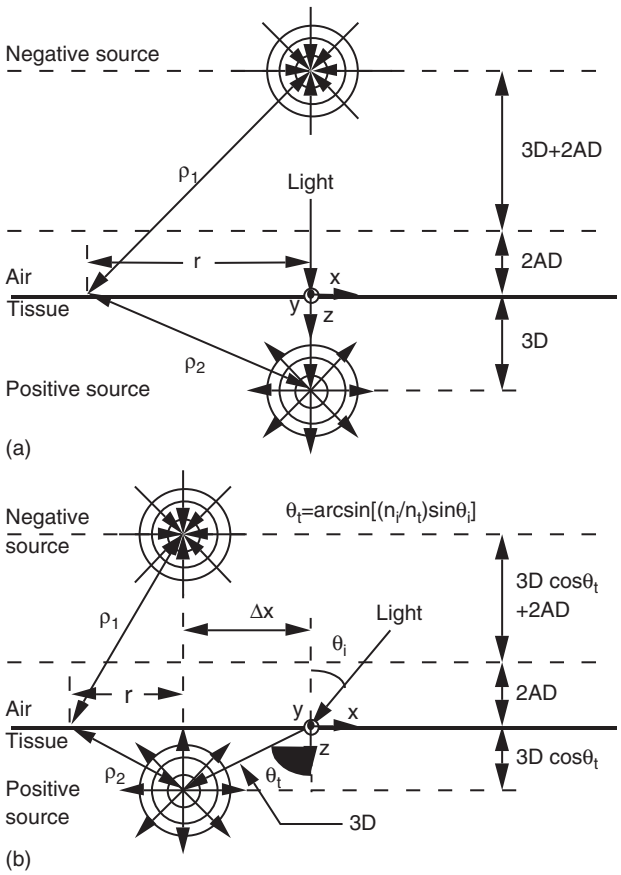

FIGURE 17.8 (a) Positions of point sources in diffusion theory model for normal incidence. (b) Positions of point sources in diffusion theory model for oblique incidence. The y-axis points out of the page. r_1 and r_2 are the distances from the positive and negative point sources to the point of interest on the tissue surface, at a radius of r from the axis of the sources. θ_t is determined from Snell's law.

The diffuse reflectance profile for oblique incidence is centered about the position of the point sources, so the shift, Δx, can be measured by finding the center of diffuse reflectance relative to the light entry point. The two source model gives the following expression:

$$R(x) = \frac{1}{4\pi}\left[\frac{\Delta z(1+\mu_{eff}\rho_1)\exp(-\mu_{eff}\rho_1)}{\rho_1^3} + \frac{(\Delta z + 2z_b)(1+\mu_{eff}\rho_2)\exp(-\mu_{eff}\rho_2)}{\rho_2^3}\right] \tag{17.45}$$

where $\Delta z = 3D\cos\theta_t$. Equation (17.45) can be scaled arbitrarily to fit a relative reflectance profile that is not in absolute units. The effective attenuation coefficient, μ_{eff}, is defined previously, while ρ_1 and ρ_2 are the distances from the two sources to the point of interest (the point of light collection; see Figure 17.8). As can be seen in Figure 17.8b, the diffusion coefficient can be calculated from Δx:

$$D = \Delta x/(3\ \sin\theta) \tag{17.46}$$

Optical properties of biological tissues depend on the tissue type and optical wavelength. For instance, the liver, with its reddish color, would have a much higher absorption coefficient from a green light source such as an argon laser than a tan piece of tissue such as chicken breast. Depending on the tissue type and exact wavelength, a typical set of optical properties for visible or near-infrared light would be 0.1 cm^{-1} for the absorption coefficient, 100 cm^{-1} for the scattering coefficient, and 0.9 for the anisotropy. In the UV region, light absorption is dominated by proteins. In the IR region, light absorption is dominated by water. The near IR (~730 nm) is considered a diagnostic window because of the minimal absorption and relatively low scattering in this region.

An important application of optical properties is the measurement of hemoglobin oxygen saturation, which is a critical physiological parameter. Because the oxygenated and deoxygenated hemoglobin molecules have different absorption spectra, the relative concentration ratio between the two forms of hemoglobin can be calculated once the optical properties of the tissue are measured.

17.3 PHYSICAL INTERACTION OF LIGHT AND PHYSICAL SENSING

After reading Section 17.2, it becomes quite apparent that most of the tissues in our bodies are not transparent to light—that is, light is typically either absorbed or scattered in tissues. In this section the physical interaction of the light with the tissue is described and its use in both sensing and therapeutics. The four fundamental physical interactions that will be described are the thermal changes induced or measured using light, pressure changes induced or measured using light, velocity changes manifested as Doppler frequency shifts in the light, and path length changes in the sample, which causes an interference pattern between two or more light beams.

17.3.1 Temperature Generation and Monitoring

All tissues in our body absorb light at various wavelengths, and the absorption process can convert the light energy into heat. In addition, our body tissues, as with any object above absolute zero temperature, also generate light radiation known as blackbody

radiation. Thus, light can be utilized to heat tissues for therapy or be measured from tissues to determine temperature.

Temperature Monitoring

The measurement of temperature, in general, has been traditionally performed reliably and fairly inexpensively using electrically based sensors such as thermistors or thermocouples. However, these sensors are not as useful when strong electromagnetic interference is present, which is common in a hospital-based setting. Also, when attempting to monitor temperature rise due to laser radiation, these sensors are inappropriate because they can absorb the laser radiation and thus can act as heat sinks. Therefore, to measure temperature in the body, several indirect optic and fiber optic approaches have been reported. For example, liquid crystal optrodes show a dramatic change with color due to temperature differences, interferometric sensors change phase or fringes with a change in the path length due to temperature variations, and the luminescence of many materials depends strongly on temperature.

The direct type of temperature sensor initially described is known as a thermographic or radiometer system. The primary application and engineering design for this type of system has been done by the military for tasks such as detecting vehicles, personnel, and even ships in total darkness. The formula for the total emission from a blackbody at temperature T is

$$I = \varepsilon \sigma T^4 \tag{17.47}$$

where ε is the emissivity and σ is the Stefan-Boltzmann constant. At room temperature, objects emit mainly in the far infrared region of the wavelength spectrum, but as temperature rises, the emission appears in the near infrared and finally in the visible spectrum. The emissivity is one ($\varepsilon = 1$) for biological tissue, and thus the total emission is dependent only on the temperature T. For the military applications, a thermographic picture generated from the IR emission can be used to display the temperature, and using this same technique, the surface temperature of the human body can be monitored for medical applications. For example, a thermal camera may be used with a TV monitor to reveal the temperature distribution on the human chest in an effort to reveal the pathologic condition of inflammation and/or breast cancer, since the affected tissue will be slightly warmer than the healthy tissue. It should be mentioned that although IR imaging is less reliable than x-ray mammography for breast screening, it is totally passive and the patients are not exposed to ionizing radiation. The thermographic systems used for this IR emission measurement require a line of sight between the warm surface and the detector. When no direct line of sight exists, an infrared-transmitting optical fiber can sometimes be used to make the connection to the detector. This type of fiber optic radiometer has been proposed for treatments using microwave heating and laser tissue heating treatments.

Light-Induced Heating

As mentioned previously, in addition to monitoring the light radiation from the body, light itself can be used to heat tissues that absorb the light. Light-induced heating of tissue can be used for a variety of applications, including biostimulation, sealing or welding

blood vessels, tissue necrosis, or tissue vaporization. Biostimulation has been claimed as a result of minute heating of the tissue whereby the light-induced heat and/or the electromagnetic field stimulates nerves and accelerates wound healing. Higher-energy absorbed laser light can facilitate the joining of tissues—in particular blood vessels (i.e., anastomosis)—or can be used to coagulate blood to stop bleeding during a surgical procedure. If the light-induced heating causes the temperature to rise above 45°C, tissue necrosis and destruction occur as would be desired for the treatment of cancer or enlarged prostate tissues. At even higher-power densities, ablation or vaporization of the tissue occurs, as is the case for the corrective eye surgery known as radial keratectomy.

The light-induced heating is typically performed with laser light. The lasers used have different wavelengths (from the ultraviolet to the infrared spectrum), power densities (i.e., ratio between beam power and irradiated area), and duration times. The amount of energy imparted to the tissue and therefore temperature rise can be changed by either varying the power density or the duration of the time pulse of the laser. For high-power densities, coagulation, necrosis, and vaporization of tissue can occur, while at low-power densities, minimal heating is observed. For some wavelengths—for instance, those of the known strong absorption bands of water—the laser beam is highly absorbed, since tissue is primarily made of water. At these wavelengths the energy is then highly absorbed in a relatively thin layer near the surface where rapid heating occurs (i.e., radial keratectomy). The absorption is less for other wavelengths used away from the water absorption bands, and this results in slower heating of a larger volume of the tissue (i.e., for prostate coagulation).

Temperature Generation and Rate of Photon Absorption

A thermodynamically irreversible mode of interaction of light with materials is the process of absorption in which the photon energy is absorbed by the material phase. In the absence of conduction, the temperature rise in tissue is governed by a thermodynamic equation of state. The equation of state requires that the change in internal energy of the system be proportional to temperature rise. The change in internal energy of the system, in the absence of conduction and other heat transfer processes, is equal to the rate of energy deposition by the laser. Expressing this relation in terms of time derivatives gives

$$\Delta U/\Delta t = \rho C \Delta T/\Delta t \approx Q_L \tag{17.48}$$

where ΔT (K) is temperature rise, Q_L (W/m^3) is volumetric rate of photon absorption by the tissue, ρ (kg/m^3) is mass density, C (J/Kg.K) is specific heat, ρC (J/m^3.K) is volumetric heat capacity, and t is the duration. A very important factor in temperature rise by photons is the rate of photon absorption Q_L, which is also known as the light/laser source term and as the rate of energy deposition. For ordinary interaction processes, the rate of absorption of photons by the material is proportional to irradiance, and the constant of proportionality is the absorption coefficient:

$$Q_L = \mu_a \phi \tag{17.49}$$

Irradiance ϕ is related to the spatial distribution of photons within the tissue.[1] For purely absorbing materials, for instance, the Beer-Lambert law applies, and if a Gaussian beam profile is additionally assumed, then

$$Q_L = \mu_a{}^*\phi_o \ \exp(-\mu_a z) \ \exp(-2r^2/\omega^2) \tag{17.50}$$

where ϕ_o is incident intensity, z is depth, and r is radial distance. In the presence of scattering, one of the scattering models discussed before can be used to describe ϕ_o.

Equation (17.48) assumes no other thermal interaction processes such as conduction, convection, or perfusion. If these processes can be ignored, as, for example, for very short laser pulses, then temperature rise can be estimated as

$$\Delta T \ \approx \ Q_L \Delta t/\rho C \tag{17.51}$$

where Δt is exposure duration. Other thermal effects of laser-tissue interaction will be considered in more detail in Section 17.5. Equation (17.51) is valid for very short irradiations during which heat diffusion is negligible. A criteria or an estimate of the upper limit for validity of Eq. (17.51) is

$$\Delta t_{MAX} = \frac{1}{\sqrt{4\mu_a^2 \alpha}} \tag{17.52}$$

where α is the thermal diffusivity of the material. For water, the value of α is about 1,400 cm^2/s.

17.3.2 Laser Doppler Velocimetry

In addition to temperature, another physical interaction of light is the Doppler phenomenon, which is based on a frequency shift due to the velocity of a moving object. For medical applications, these objects are typically the moving red blood cells with a diameter of roughly 7 μm. The Doppler approach is used for measuring blood flow velocity for a variety of medical applications, including heart monitoring, transluminar coronary angioplasty, coronary arterial stenosis, tissue blood flow on the surface of the body, and monitoring blood flow on the scalp of a fetus during labor.

When a light wave of frequency f and velocity c impinges on a stationary object, it is reflected at the same frequency. However, if the object moves with velocity v, the reflected frequency f' is different from f. This difference or shift in frequency, δf, from the original light wave is known as the Doppler effect or Doppler shift and can be described as

$$\delta f = f - f' \tag{17.53}$$

The Doppler shift is described in Eq. (17.54) in terms of the velocity, v, of the moving red blood cells, the refractive index of the medium, n, the speed of light in the tissue, c_o, the input frequency, f, and the angle between the incident beam and the vessel, θ:

$$\delta f/f = 2 \ v \ n \ \cos\theta/c_o \tag{17.54}$$

[1]For multiphoton light-tissue interaction processes, the exponent of ϕ is increased. For example, for a two-photon process $Q_L = \mu_a * \phi^2$.

Further, it is well known that the wavelength, λ, is equal to the speed of light divided by the frequency, so

$$\delta f = 2\, v\, n\, \cos\theta/\lambda_o \tag{17.55}$$

A comparable analogy for the Doppler effect with sound waves is a train moving toward an observer. As the train gets closer, the whistle sounds like a higher pitch.

EXAMPLE PROBLEM 17.7

Using a laser Doppler system, calculate the velocity of blood given an argon laser (514 nm) at an angle with the vessel of 30 degrees, an index of refraction of 1.33, and a frequency shift of 60 KHz. Does this make sense physiologically? Does it really matter if you were off in your probe to vessel measurement angle by 10 degrees?

Solution

Using Eq. (17.55), the velocity can be calculated to be

$$v = (\delta f^{*}\lambda)/(2n\, \cos(\theta)) = [(60 \times 10^{3})(514 \times 10^{-9})]/[2\, (\cos(30))\, (1.33)] = 1.34\ \text{cm/s}$$

This is reasonable for an average-sized vessel in the human body. If you were off by 10 degrees—for example, if you thought the angle was 40 instead of 30—this would make a pretty big difference with the newly calculated speed of 1.51 cm/s (a 13 percent error).

Laser Doppler is a good method for monitoring velocities, but one reason it has not gained wide use clinically is that the flow (cm^3/sec) of blood or rather the average velocities of all the particles in the fluid is the physical quantity of diagnostic value, and flow cannot be directly measured using the Doppler approach. Calculating the flow rate for a rigid tube filled with water by knowing the velocity is a straightforward problem to solve. However, determining the absolute flow rate of blood in the body by simply using the Doppler measured velocity is a much more difficult problem, particularly for narrow vessels. Blood is thicker than water, and the flow characteristics are more complex. Blood vessels are also not rigid, straight tubes, and the flow of blood is pulsatile. Finally, a fiber optic probe can be inserted in the blood vessel and scanned to get a series of velocity measurements to determine flow, but the probe itself can alter the flow measurement.

Overall, laser Doppler velocimetry is a simple concept that can, with some effort, be used to measure relative changes in flow, but it is very difficult for this approach to be calibrated for absolute flow measurements. Thus, the standard for blood mass-flow measurements has been by thermodilation and is widely used in clinical practice. The thermodilation method is used to determine flow by inducing a predetermined change in the heat content of the blood at one point of the circulation and detecting the resultant change in temperature at some point downstream, after the flow has caused a controlled degree of mixing across the vessel diameter.

17.3.3 Interferometry

The phenomenon of interference is another method by which physical light interaction takes place, and it depends on the superposition of two or more individual waves, typically originating from the same source. Since light consists of oscillatory E and M fields that are

vectors, they add vectorally. Thus, when two or more waves emanating from the same source are split and travel along different paths, they can then reunite and interfere constructively or destructively. When the constructive and destructive interferences are seen to alternate in a spatial display, the interference is said to produce a series or pattern of fringes. If one of the paths in which the light travels is altered by any small perturbation, such as that due to temperature, pressure, or index of refraction changes, then once recombined with the unaltered reference beam, the perturbation causes a shift in the fringe pattern that can be readily observed with optoelectronic techniques to about 10^{-4} of the fringe spacing. The useful information regarding the changing variable of interest can be measured quite accurately as a path length change on the order of one-hundredth of a wavelength or 5×10^{-9} meters for visible light.

There are several variations for producing light interference, including one of the first instruments known as the Rayleigh refractometer from which came the Mach-Zehnder interferometer. For the sake of brevity, this section focuses on two more sophisticated variations of the Rayleigh idea: the dual beam Michelson interferometer and the multiple beam Fabry-Perot interferometer. As shown in Figure 17.9, the Michelson interferometer begins with a light source that is split into two beams by means of a beam-splitting mirror or fiber optics, which also serves to recombine the light after reflection from fully silvered mirrors. A compensating plate is sometimes needed to provide equal optical paths before introduction of any perturbation or sample to be measured. The perturbation can take the form of a pressure or temperature change, causing a strain and thus a path length change in the sample arm of the fiber optic or as a change due to the addition of a tissue sample or replacement of the mirror with a tissue sample. For example, the Michelson interferometer has been investigated for measuring tissue thickness, particularly for corneal tissue as feedback for the radial keratectomy procedure (laser removal or shaving of the cornea to correct vision), and this interferometer, when used with a low coherent light source, has been researched for use in optical coherence tomographic imaging of superficial tissues. The governing equation for the irradiance of the fringe system of circles concentric with the optic axis in which the two interfering beams are of equal amplitude is given as

$$I = 4I_o \cos^2(\delta/2) \tag{17.56}$$

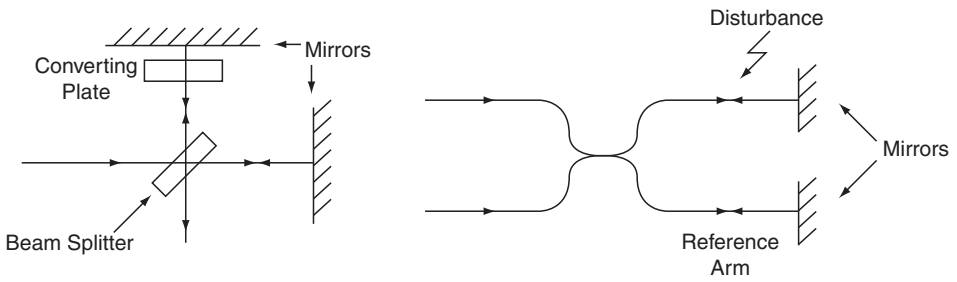

FIGURE 17.9 Michelson interferometer: (a) bulk optics and (b) fiber optics.

where I_o is the input intensity and the phase difference δ is defined as

$$\delta = 2\pi\Delta/\lambda \tag{17.57}$$

In this equation, λ is the wavelength, and the net optical path difference, Δ, is defined as

$$\Delta = 2d\cos(\theta) + \lambda/2 = (m + 0.5)\lambda \tag{17.58}$$

Clearly, from Eq. (17.58) the following equation can be derived

$$2d\cos(\theta) = m\lambda \tag{17.59}$$

in which $2d$ is the optical path difference or, rather, the difference in the two paths from the beam splitter, m is the number of fringes, and θ is the angle of incidence ($\theta = 0$ is a normal or on-axis beam). When a plate, a gas, or a thin minimally absorbing or scattering tissue slice is assumed with constant index of refraction and is inserted in one of the paths, then $d = (n_s - n_{air})L$, in which L is the actual length of the substance, n_s is the index of refraction of the substance, and n_{air} is the index of refraction of the air.

EXAMPLE PROBLEM 17.8

A thin sheet of clear tissue, such as a section of the cornea of the eye ($n \approx 1.33$), is inserted normally into one beam of a Michelson interferometer. Using 589 nanometers of light, the fringe pattern is found to shift by 50 fringes. Determine the thickness of the tissue section.

Solution

From Eq. (17.59), $2d\cos(\theta) = m\lambda$, and thus $d = (50\times.589)/2 = 14.72$ micrometers, which is the calculated optical path length. However, the physical length of the tissue must take into account the index of refraction of the sample and the air. Thus, as described in the paragraph after Eq. (17.59), the equation for physical path length is $L = d/(n_s - n_{air}) = 14.72/(1.33 - 1.0) = 44.6$ micrometers.

All the dual beam interferometry techniques such as the Michelson and Mach-Zehnder approaches suffer from the limitation that the accuracy depends on the location of the maxima (or minima) of a sinusoidal variation, as shown in Eq. (17.59). For very accurate measurements, such as precision spectroscopy, this limitation is severe. Rather than a dual beam, if the interference of many beams is utilized, the accuracy can be improved considerably. A Fabry-Perot interferometer uses a multiple beam approach, as shown in Figure 17.10. As can be seen in the figure, the interferometer uses a plane parallel plate to produce an interference pattern by combining the multiple beams of the transmitted light. The parallel plate is typically composed of two thick glass or quartz plates that enclose a plane parallel plate of air between them. The flatness and reflectivity of the inner surfaces are important and are polished generally better than λ/50 and coated with a highly reflective layer of silver or aluminum. The silver is good for wavelengths above 400 nm in the visible light region, but aluminum has better reflectivity below 400 nm. These film coatings must also be thin enough to be partially transmitting (~50 nm thickness for silver coatings). In many instances the outer surfaces of the glass plate are purposely formed at a small angle relative to the inner faces (several minutes of arc) to eliminate spurious fringe

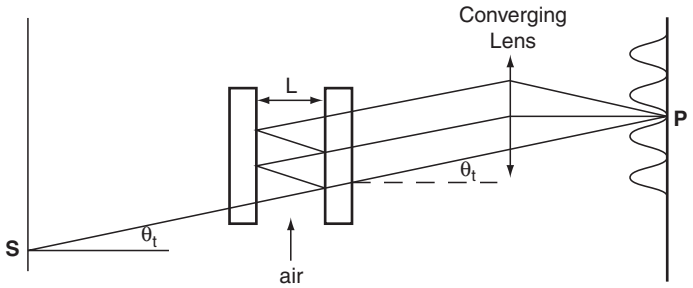

FIGURE 17.10 Fabry-Perot multiple beam interferometer.

patterns that can arise from the glass itself acting as the parallel plate interferometer. When L is fixed, the instrument is referred to as a Fabry-Perot etalon. The nature of the superposition at point P is determined by the path difference between successive parallel beams, so

$$\Delta = 2n_f\, L\, \cos\theta_t = m\lambda_{(\text{minimum})} = 2L\, \cos\theta_t \tag{17.60}$$

using $n_f = 1$ for air.

Other beams from different points of the source but in the same plane and making the same angle θ_t with the axis satisfy the same path difference and also arrive at P. With L fixed, Eq. (17.60) for Δ is satisfied for certain angles θ_t and the fringe system is the familiar concentric rings due to the focusing of fringes of equal inclination, as shown in Figures 17.11a and b. If the thickness of L varies with time, a detector D will record an interferogram as a function of time, as shown in Figure 17.11c.

Variation in the fringe pattern irradiance of the Fabry-Perot as a function of phase or path difference is known as the fringe profile. The sharpness of the fringes is important to the ultimate resolving power of the instrument. Using the trig identity $\cos\delta = 1 - 2\sin^2(\delta/2)$, the transmittance can be written as

$$T = I_T/I_i = 1/(1 + [4r^2/(1-r^2)^2]\, \sin^2(\delta/2)) \quad \text{(Airy function)} \tag{17.61}$$

where r is the reflectivity, and the term in the square brackets in the denominator is known as the coefficient of finesse, F, and thus,

$$T = 1/(1 + F\, \sin^2(\delta/2)) \tag{17.62}$$

It should be noted that as $0 < r < 1$, then $0 < F < \infty$. The coefficient of finesse, F, also represents a certain measure of fringe contrast:

$$F = ((I_T)_{\max} - (I_T)_{\min})/I_{T\,\min} = (T_{\max} - T_{\min})/T_{\min} \tag{17.63}$$

It should be noted here that $T_{\max} = 1$ when $\sin(\delta/2) = 0$, and $T_{\min} = 1/(1 + F)$ when $\sin(\delta/2) = \pm 1$. Given r, the fringe profile can be plotted as shown in Figure 17.12. As seen in the figure, $T = T_{\max} = 1$ at $\delta = m2\pi$ and $T = T_{\min} = 1/(1 + F)$ at $\delta = (m + ½)2\pi$. Further, $T_{\max} = 1$ regardless of r, and $T_{\min}$ is never zero but approaches zero as r approaches one. Also, the transmittance peaks sharply at higher values of r, remaining near zero for most of the region between the fringes. It should be noted that the Michelson interferometer

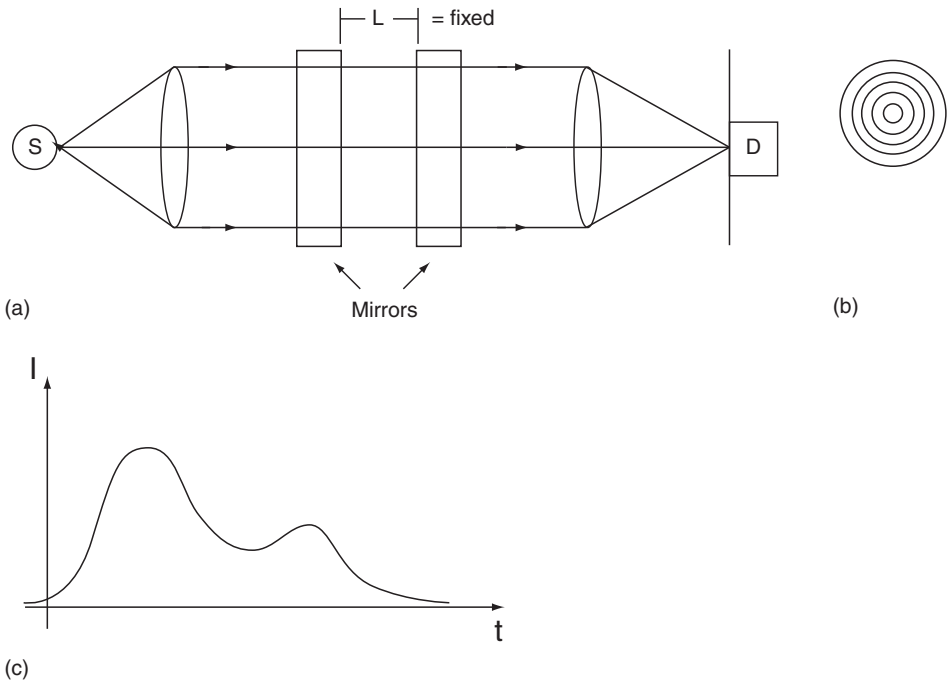

FIGURE 17.11 F-Petalon with L fixed.

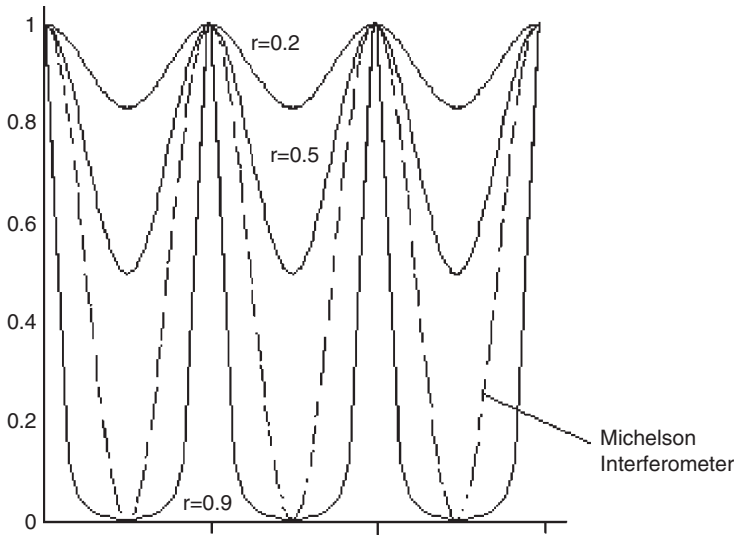

FIGURE 17.12 The difference in resolution between the multiple beam Fabry-Perot interferometer with different reflectivities and the dual beam Michelson interferometer.

produces broad fringes when it is normalized to the same max value, since it has a simple $\cos^2(\delta/2)$ dependence on the phase (dashed lines in the figure). An example of a fiber optic–based Fabry-Perot interferometer is the commercially available intracranial fluid pressure monitoring system for patients with severe head trauma or hydrocephalus (increased amount of cerebral spinal fluid in the ventricles and/or subarachnoid spaces of the brain).

17.4 BIOCHEMICAL MEASUREMENT TECHNIQUES USING LIGHT

In the last few years, there has been much enthusiasm and considerable effort from medical device companies and universities to perform diagnostic procedures such as cancer detection and quantifiably monitor blood chemicals, such as glucose, lactic acid, albumin, and cholesterol using various optical approaches. The most well-known optical monitoring approach used clinically in vivo is the pulse oximeter, which indirectly measures oxygen saturation and changes in blood volume by detecting changes in the optical absorption peaks of oxygenated and deoxygenated hemoglobin as it is pulsed through the arteries. It is often used to also measure heart rate.

The most common optical approaches for diagnostic and sensing applications include absorption, scattering, luminescence, and polarimetry. The primary variable for each of these approaches is a change in the light intensity as it passes through the medium, which can change as a function of the wavelength or polarization of the light. The lifetime and/or phase can also be used as a variable. For absorption and luminescence, the intensity will change nearly linearly for moderate analyte concentrations and nonlinearly for high concentrations.

17.4.1 Spectroscopic Measurements Using Light Absorption

Many investigators have suggested infrared absorption as a potential route to blood chemical monitoring and diagnostic sensing, in particular for glucose monitoring and cancer detection. The governing Eq. (17.17) for purely absorbing media as well as fluorescence was described previously using the Beer-Lambert law. Expressed logarithmically, the equation becomes

$$A = \ln(T) = \ln(I_o/I) = \mu\, z = z\, \Sigma\, \varepsilon_i\, C_i \tag{17.64}$$

in which A is absorbance, T is transmittance, I_o is the incident light, I is the transmitted light, z is the path length, and μ is the absorption coefficient, or rather the sum of the multiplication of the molar absorptivity times the concentration of all the different components in the analyte. For tissue and blood this equation is valid in the midinfrared wavelength region (wavelengths of 2.5–12 micrometers), in which the absorption peaks due to various chemicals are distinguishably sharp and the scatter is weak. Unfortunately, the absorption of the light due to water within tissue in this region is orders of magnitude stronger than any of the blood chemicals, which results in the possibility of only short path length sample investigations (on the order of micrometers). This brings about the possibility for surface or superficial investigations on the skin or, with the use of fiber optics, on internal body

cavities. Unfortunately, the optical fibers available in this region tend to be toxic, hydroscopic, and/or rigid. Consequently, the combination of the water absorption and lack of good fibers makes in vivo diagnostics and sensing very difficult in the mid-IR region. The light sources used in this region include the broad-based tungsten bulb, nernst glower, nichrome wire, and globar rod, and narrowly tunable, typically liquid nitrogen cooled, laser diodes. The detectors used include the cooled mercury cadmium telluride (MCT), thermopile, and thermistor. The optics include sodium chloride and potassium bromide, mirrors (typically gold coated), and gratings.

In the near-infrared (NIR) wavelength region, the spectrum is not affected by water to the same degree as the midinfrared region, allowing for path lengths within the tissue of 1 mm to 1 cm to be used. In addition, low OH silica fibers are quite transparent across this range and are nontoxic and nonhydroscopic. The NIR region (700–2,500 nm) exhibits absorptions due to low-energy electronic vibrations (700–1,000 nm), as well as overtones of molecular bond stretching and combination bands (1,000–2,500 nm). These bands result from interactions between different bonds (−CH, −OH, −NH) to the same atom. Typically, only the first, second, and third overtones of a molecular vibration are detectable and are broad in nature. Thus, only at high concentrations of the chemical species are these overtones qualitatively detectable with the intensity dropping off rapidly as overtone order increases. The NIR absorption bands are also influenced by temperature, pressure, and hydrogen bonding effects and can overlap significantly. In the 700 to 1,200 nm region, they are also influenced by scattering effects. Thus, unlike mid-IR spectroscopy, NIR spectroscopy is primarily empirical and not well suited for qualitative work. However, using techniques such as multivariate statistics, quantitative analysis is possible with the NIR spectrum. The light sources used in this region include the broad-based tungsten bulb, light emitting diodes (LEDs), laser pumped solid-state lasers such as the tunable titanium sapphire laser, and laser diodes. The detectors used include silicon (good to 1 micrometer), germanium (good to 1.7 micrometers), and indium antiminide (good to 5.5 micrometers). The optics include low OH glasses, quartz, glass, gratings, and mirrors.

The means for separating the wavelength of the light of a broadband source include dispersive and nondispersive methods. The dispersive approach uses either a ruled reflective grating or transmissive prism to separate the wavelengths of light. The nondispersive systems include a series of wavelength selection filters or a Fourier transform infrared (FTIR)-based instrument. The FTIR method uses an interferometer similar to the Michelson interferometer shown in Figure 17.9 to collect the entire spectrum and then deconvolutes it, using Fourier transform techniques. Both approaches can be configured to cover the NIR and mid-IR ranges. The advantages of the dispersive systems include higher resolution and separation of closely spaced wavelength bands, while the nondispersive systems generally have better throughput, since all the light passes through the sample.

17.4.2 Monitoring Approaches Using Scattered Light

There are fundamentally two types of optical scattering for diagnostics and monitoring: elastic and inelastic. The elastic scattering can be described using Mie theory (or Rayleigh scattering for particles that are small compared to the wavelength), in which the intensity of the scattered radiation can be related to the concentration, size, and shape of the

scattering particles. The inelastic scattering, in which the polarization of the particle is not constant, can be described as Raman scattering. Note that fluorescence, although an absorption reemission process, is also inelastic.

When using the light scattering phenomenon for sensing, the intensity of the reflected light is usually considered. The reflection of light, however, can be divided into two forms. Specular reflection, or a "mirror" type of reflection, occurs at the interface of a medium. The returned light yields little information about the material other than its roughness, since it never penetrates the medium. Thus, for applications other than surface roughness, the specularly reflected light is typically minimized or eliminated with the design of the optical sensor. Diffuse reflection, however, occurs when light penetrates into a medium, becomes absorbed and multiply scattered, and makes its way back to the surface of the medium. The model describing the role of diffuse scattering in tissue is based on the radiative transfer theory, as was described in Section 17.2. The same theory applies for sensing as well.

The use of elastically scattered light has been suggested for both diagnostic procedures such as cancer detection and for monitoring analytes such as glucose noninvasively for diabetics. For use as a monitoring application of chemical changes such as glucose, researchers have used an intensity-modulated frequency domain NIR spectrometer, capable of separating the reduced scattering and absorption coefficients to detect changes in the reduced scattering coefficient showing correlation with blood glucose in human muscle. This approach was promising at first as a relative measure over time, since clearly an increase in glucose concentration in the physiologic range decreases the total amount of tissue scattering. However, the drawbacks of the light elastic scattering approach for analyte monitoring are still quite daunting. The specificity of the elastic scattering approach is the biggest concern with this method, since other physiologic effects unrelated to glucose concentration could produce similar variations of the reduced scattering coefficient with time, and unlike the absorption approach, elastic light scattering as a function of the molecule is nearly wavelength independent.

The measurement precision of the reduced scattering coefficient and separation of scattering and absorption changes is another concern with this approach. It is difficult to measure such small changes and be insensitive to some of the larger absorption changes in the tissue, particularly hemoglobin. This approach also needs to take into account the different refractive indices of tissue. Tissue scattering is caused by a variety of substances and organelles (membranes, mitochondria, nuclei, etc.), and all of them have different refractive indices. The effect of blood glucose concentration and its distribution at the cellular level is a complex issue that needs to be investigated before this approach can be considered viable. An instrument of this type would require in vivo calibration against a gold standard, since the reduced scattering coefficient is dependent on additional factors such as cell density. Last, there is a need to account for factors that might change the reduced scattering coefficient, such as variations in temperature, red blood cell concentration, electrolyte levels, and movements of extracellular and intracellular water.

As a diagnostic screening tool for cancer detection, measurement of the scatter in thin tissues or cells may hold promise. Many of the changes in tissue due to cancer are morphologic rather than chemical and thus occur with changes in the size and shape of the cellular and subcellular components (membranes, mitochondria, nuclei, etc.). Thus, the changes in elastic light scatter should be larger with the morphologic tissue differences.

If the wavelength of the elastic light scattering is carefully selected so as to be outside the major absorption areas due to water and hemoglobin and if the diffusely scattered light is measured as a function of angle of incidence, there is potential for this approach to aid in pathologic diagnosis of disease.

Inelastic Raman spectroscopic scattering has been utilized over the past few decades initially by physicists and chemists. Raman spectroscopy has become a powerful tool for studying a variety of biological molecules, including proteins, enzymes and immunoglobulins, nucleic acids, nucleoproteins, lipids and biological membranes, and carbohydrates, but with the advent of more powerful laser sources and more sensitive detectors, it has also become useful as a diagnostic and sensing tool. The phenomenon of Raman scattering is observed when monochromatic (single wavelength) radiation is incident upon the media. In addition to the elastic scatter of the transmitted light, a portion of the radiation is inelastically scattered. Thus, some of the incident light of frequency w_o exhibits frequency shifts $\pm w_m$, which is associated with transitions between rotational, vibrational, and electronic levels that are specific to a particular analyte of interest. Most studies utilize the Stokes type of scattering bands that correspond to the $w_o - w_m$ scattering. Therefore, the Raman bands typically used are those shifted by the interaction with the analyte to longer wavelengths relative to the excitation wavelength.

As with infrared spectroscopic techniques, Raman spectra can be utilized to identify molecules, since these spectra are characteristic of variations in the molecular polarizability and dipole moments. Raman spectroscopy can be considered as complementary to absorption spectroscopy because neither technique alone can resolve all of the energy states of a molecule. In fact, for certain molecules, some energy levels may not be resolved by either technique. Due to the anharmonic oscillator model for dipoles, overtone frequencies exist in addition to fundamental vibrations. It is an advantage of Raman spectroscopy that the overtones are much weaker than the fundamental tones, thus contributing to simpler spectra as compared to absorption spectroscopy.

One advantage to using Raman spectroscopy in biological investigations is that the Raman spectrum of water is weaker and therefore, unlike infrared spectroscopy, only minimally interferes with the spectrum of the solute. Thus, the spectrum can be obtained from aqueous solutions at reasonable path lengths. However, the Raman signal is also weak, and only recently, with the replacement of slow photomultiplier tubes with faster CCD arrays as well as the manufacture of higher power near infrared laser diodes, has the technology become available to allow researchers to consider the possibility of distinguishing normal and abnormal tissue types as well as quantifying blood chemicals in near real time. In addition, investigators have applied statistical methods such as partial least squares (PLS) to aid in the estimation of biochemical concentrations from Raman spectra.

As with elastic scatter, Raman spectroscopy has been used for both diagnostics and monitoring. The diagnostic approaches look for the presence of different spectral peaks and/or intensity differences in the peaks due to different chemicals present in, for instance, cancerous tissue. For quantifiable monitoring it is the intensity differences alone that are investigated. In tissue, one problem is the high fluorescence background signal as a result of autofluorescence incurred in heavily vascularized tissue due to the high concentration of proteins and other fluorescent components. Instrumentation to excite in the NIR

wavelength range has been proposed to overcome the autofluorescence problem, since the fluorescence component falls off with increasing wavelength.

Excitation in the NIR region offers the added advantage of longer wavelengths that pass through larger tissue samples with lower absorption and scatter than other spectral regions, such as visible or ultraviolet. However, in addition to fluorescence falling off with wavelength, the Raman signal also falls off to the fourth power as wavelength increases. Thus, there is a tradeoff between minimizing fluorescence and maintaining the Raman signal. The eye has been suggested as a site for analyte concentration measurements using Raman spectroscopy to minimize autofluorescence, but the disadvantage to using the eye for Raman spectroscopy is that the laser excitation powers must be kept low to prevent injury and this significantly reduces the signal-to-noise ratio. Finally, like infrared and NIR absorption, to quantifiably determine the inherently low concentrations of analytes in vivo, the presence of different chemicals must be accounted for that yield overlapping Raman spectra.

17.4.3 Use of the Luminescence Property of Light for Measurement

As described previously, luminescence is the absorption of photons of electromagnetic radiation (light) at one wavelength and reemission of photons at another wavelength. The photons are absorbed by the molecules in the tissue or medium, raising them to some excited energy state, and then, upon returning to a lower energy state, the molecules emit radiation or, rather, luminesce at a different wavelength. The luminescent effect can be referred to as fluorescence or phosphorescence. Fluorescence is luminescence that has energy transitions that do not involve a change in electron spin, and therefore the reemission occurs much faster. Consequently, fluorescence occurs only during excitation, while phosphorescence can continue after excitation (i.e., after the light source is turned off). As an example, a standard television while turned on is producing fluorescence, but for a very short time after it is turned off the screen will phosphoresce.

The measurement of fluorescence has been used for diagnostic, monitoring, and research purposes. Fluorescent microscopes are now being used for research that produce outstanding images of cells and tissues that provide a variety of information about them. Obtaining diagnostic information, in particular with respect to cancer diagnosis or the total plaque in arteries, has also been attempted using both intrinsic fluorescence of tissue and extrinsic dyes. The intrinsic fluorescence is due to the naturally occurring proteins, nucleic acids, and nucleotide coenzymes within the tissue, while extrinsic fluorescence is induced by the uptake of certain dyes in the tissue. Extrinsic fluorescence has also been investigated, for instance, to monitor such analytes as glucose, intracellular calcium, proteins, and nucleotide coenzymes. Unlike the use of fluorescence in chemistry on dilute solutions, the intrinsic or autofluorescence of tissue, as well as the scattering and absorption of the tissue, acts as a noise source for the extrinsic approach.

The response of a fluorescence sensor can be described in terms of the output intensity as

$$I_f = \Phi_f \, (I_o - I) \tag{17.65}$$

in which I_f is the radiant intensity of fluorescence, Φ_f is the fluorescence efficiency, I_o is the radiant intensity incident on the sample, and I is the radiant intensity emerging from the

sample. The fluorescence efficiency can be described as the combination of three factors. First is the quantum yield, which is the probability that an excited molecule will decay by emitting a photon rather than by losing its energy nonradiatively. This parameter varies from 1.00 to 0.05 and varies with time on the order of nanoseconds. Thus, in addition to intensity measurements, time-resolved fluorescence measurements are possible using pulsed light sources and fast detectors. The second parameter is the geometrical factor, which is the solid angle of fluorescence radiation subtended by the detector and that depends on your probe design. Last is the efficiency of the detector itself for the emitted fluorescence wavelength.

Since fluorescence is an absorption/reemission technique, it can be described in terms of Beer's law as

$$I_f = \Phi_f \, I_o \, [1 - \exp(-\varepsilon C l)] \tag{17.66}$$

in which C is the concentration of the analyte, l is the path length, and ε is the molar absorptivity. Equation (17.66) can be described in terms of a power series, and for weakly absorbing species ($\varepsilon C l < 0.05$) only the first term in the series is significant. Therefore, under these conditions, the response of the fluorescence sensor becomes linear with analyte concentration and can be described as

$$I_f = \Phi_f \, I_o \, \varepsilon C l \tag{17.67}$$

The primary fluorescent sensors are based on the measurement of intensity, but lifetime measurements in the time or frequency domain are also possible. To gain the most information, particularly in a research or teaching setting, dual monochromators (grating-based wavelength separation devices) are used with either a photomultiplier tube as the detector or a CCD array detector. In a typical benchtop fluorimeter, a broad, primarily ultraviolet/visible xenon bulb is used as the light source. The light is coupled first through a monochromator, which is a wavelength separator that can be set for any excitation wavelength within the range of the source. The light then passes through the sample and is collected by a second monochromator. The light reflected from the grating within the second monochromator can be scanned so a photomultiplier tube (PMT) receives the different wavelengths of light as a function of time. Alternatively, all the wavelengths from the grating can be collected simultaneously on a CCD detector array.

The advantage of the CCD array is that it provides for real-time collection of the fluorescence spectrum. The advantage of the PMT is that it is typically a more sensitive detector. In many systems a small portion of the beam is split at the input and sent to a reference detector to allow for correction of fluctuations in the light source. Once the optimal configuration for a particular biomedical application, such as cervical cancer detection or glucose sensing, has been investigated using the benchtop machine, an intensity measurement system can be designed with a simpler, more robust configuration. Such a system can be designed with lasers and/or wavelength-specific filters instead of monochromators and be made to work at two or more discrete wavelengths. In addition, optical fibers can be used for delivery and collection of the light to the remote area. Since the excitation wavelength and fluorescent emission wavelengths are different, the same fiber or fibers can be used to both deliver and collect the light. In any configuration it is important to match the spectral characteristics of

the source, dye if used, sample, and detector. For instance, depending on the tissue probed, there are strong absorbers, scatterers, and autofluorescence that need to be factored into any fluorescent system design.

17.4.4 Measurements Made Using Light Polarization Properties

Having discussed some of the fundamental electromagnetic theory of polarized light generation in Section 17.1.2, some of the applications of polarized light shall now be discussed. Applications of polarized light include biochemical quantification in vivo such as noninvasively monitoring glucose for diabetes, measuring birefringence in tissues using polarized light microscopy, and tissue characterization, in particular to aid in cancer identification or for use in the measurement of the nerve fiber layer of normal and glaucomatous eyes.

The rotation of linearly polarized light by optically active substances has been used for many years to quantify the amount of the substance in solution. A variety of both polarimeters, adapted to the examination of all optically active substances, and saccharimeters, designed solely for polarizing sugars, have been developed. The concept behind these devices is that the amount of rotation of polarized light by an optically active substance depends on the thickness of the layer traversed by the light, the wavelength of the light used for the measurement, the temperature, the pH of the solvent, and the concentration of the optically active material.

Historically, polarimetric measurements have been obtained under a set of standard conditions. The path length typically employed as a standard in polarimetry is 10 cm for liquids, the wavelength is usually that of the green mercury line (5,461 Angstroms), and the temperature is 20°C. If the layer thickness in decimeters is L, the concentration of solute in grams per 100 ml of solution is C, α is the observed rotation in degrees, and $[\alpha]$ is the specific rotation or rotation under standard conditions, which is unique for all chiral molecules, then

$$C = \frac{100\alpha}{L[\alpha]} \tag{17.68}$$

In the preceding equation, the specific rotation $[\alpha]$ of a molecule is dependent on temperature, T, wavelength, λ, and the pH of the solvent.

For polarimetry to be used as a noninvasive technique—for instance, in blood glucose monitoring—the signal must be able to pass from the source, through the body, and to a detector without total depolarization of the beam. Since the skin possesses high scattering coefficients, which causes depolarization of the light, maintaining polarization information in a beam passing through a thick piece of tissue (i.e., 1 cm), which includes skin, would not be feasible. Tissue thicknesses of less than 4 mm, which include skin, may potentially be used, but the polarimetric sensing device will encounter greater than 95 percent depolarization of the light due to scattering from the tissue.

As an alternative to transmitting light through the skin, the aqueous humor of the eye has been investigated as a site for detection of in vivo glucose concentrations, since this sensing site is a clear biological optical media. It is also known that glucose concentration of the aqueous humor of the eye correlates well with blood glucose levels, with a minor

time delay (on the order of minutes) in rabbit models. The approximate width of the average anterior chamber of a human eye is on the order of 1 cm. Therefore, an observed rotation of about 4.562 millidegrees per optical pass can be expected for a normal blood glucose level of 100mg/100ml, given a specific rotation of glucose at $\lambda = 633$ nm of $45.62^{\circ}\text{cm}^2\text{g}^{-1}$ and thickness of 1 centimeter. The eye as a sensing site, however, is not without its share of potential problems. For instance, potential problems with using the eye include corneal birefringence and eye motion artifact.

As shown in Eq. (17.68), the rotation is directly proportional to the path length, and thus it is critical that this length be determined or at least kept constant for each individual subject regardless of the sensing site. If the eye is used as the sensing site, the angle of incidence on the surface of the cornea must be kept relatively constant for each patient so not only the path length but alignment remains fixed each time a reading is taken. In most tissues, including the eye, the change in rotation due to other chiral molecules such as proteins needs to be accommodated in any final instrument. In addition, most other tissues also have a birefringence associated with them that would need to be accounted for in a final polarimetric glucose sensor.

It is the birefringence and retardation of the polarized light as well as polarized scattering of the tissue that are the signals rather than the noise when using polarized light for tissue characterization. For example, a scanning laser polarimeter has been used to measure changes in retardation of the polarized light impinging on the retinal nerve fiber layer. It has been shown that scanning laser polarimetry provides statistically significant higher retardation for normal eyes in certain regions over glaucoma eyes. Images generated from the scattering of various forms of polarized light have also been shown to be able to differentiate between cancer and normal fibroblast cells.

17.4.5 Micrometer and Nanometer Biosensing Applications

Developments in microtechnology and, in particular, nanotechnology are transforming the fields of biosensors, prosthesis and implants, and medical diagnostics. In terms of medical diagnostics, these devices are being used in combination with optical biosensing for external, lab-on-a-chip, high-throughput screening for analyzing blood and other samples. Inside the body many researchers and companies are developing optically based nanotechnology applications for cancer diagnosis and therapy.

One nanotechnology used in biomedical optics that has come to the forefront is that of quantum dots. Quantum dots are devices capable of confining electrons in three dimensions in a space small enough that their quantum (wave-like) behavior dominates over their classical (particle-like) behavior. At room temperature, confinement spaces of 20–30 nm or smaller are typically required. Once the electrons are confined, they repel one another, and no two electrons can have the same quantum state. Thus, the electrons in a quantum dot will form shells and orbitals highly reminiscent of the ones in an atom, and will exhibit many of the optical, electrical, thermal, and chemical properties of an atom. Quantum dots can be grown chemically as nanoparticles of semiconductor surrounded by an insulating layer nearly colloidal in nature. These particles can also be deposited onto a substrate, such as a semiconductor wafer patterned with metal electrodes, or they can be crystallized into bulk solids by a variety of methods. Either substance can be stimulated with electricity or

light (e.g., lasers) in order to change its properties. Fundamentally, when you excite a quantum dot with one wavelength, depending on the size of the dot, it will emit (fluoresce) at a narrow-band longer wavelength. The size-dependent behavior allows them to be used for multiplexing, since a single wavelength can be used to excite different-sized quantum dots to produce multiple wavelengths within a sample.

Although quantum dots are nanometer-scale crystals that were developed in the mid-1980s for optoelectronic applications, one application in the biomedical area has been to probe living cells in full color over extended periods of time. Such a technique could reveal the complex processes that take place in all living organisms in unprecedented detail, such as the development of embryos. Existing imaging techniques use natural molecules that fluoresce, as just discussed, such as organic dyes and proteins that are found in jellyfish and fireflies. However, each dye emits light over a wide range of wavelengths, which means that their spectra overlap, and this makes it difficult to use more than three dyes at a time in order to tag and image different biological molecules simultaneously. The fluorescence of dyes also tends to fade away quickly over time, whereas semiconductor nanocrystals—quantum dots—can get around these problems. In addition to being brighter and lasting longer than organic fluorophores, quantum dots have a broader excitation spectrum and thus, as mentioned, a mixture of quantum dots of different sizes can be excited by a light source with a single wavelength, allowing simultaneous detection and imaging in color.

Although the preceding example has focused on biomedical sensing using fluorescent quantum dots, these micro- and nanoparticles can also be made of various materials and used with all of the preceding light propagation methods. For instance, metal nanoparticles such as gold or silver can be used with Raman spectroscopy to produce an effect known as surface-enhanced Raman spectroscopy (SERS), which gives rise to signals a million times more sensitive than regular Raman signals. These same types of metal nano- or microparticles can be injected into cancerous tissue and used as absorbers that when hit with infrared light will absorb the energy, cook the cancerous tumor, and kill it. Since nanoparticle development is still in its infancy, where they go in the body, their toxicology, whether they can be functionalized to go to specific organs or cells like cancer, and what other biomedical applications are to come from the combination of these particles with light remain to be seen.

17.5 FUNDAMENTALS OF THE PHOTOTHERMAL THERAPEUTIC EFFECTS OF LIGHT SOURCES

The therapeutic application of light, including lasers, is mediated by conversion of photonic energy to absorbed energy within the material phase of the tissue. The primary mode of this energy conversion manifests itself as a nonuniform temperature rise that leads to a series of thermodynamic processes. These thermodynamic processes can then be exploited as a means to affect therapeutic actions such as photothermal coagulation and ablation of tissue. Another mode of interaction is the utilization of the absorbed energy in activation of endogeneous or exogenous photosensitizing agents in a photochemical process known as photodynamic therapy.

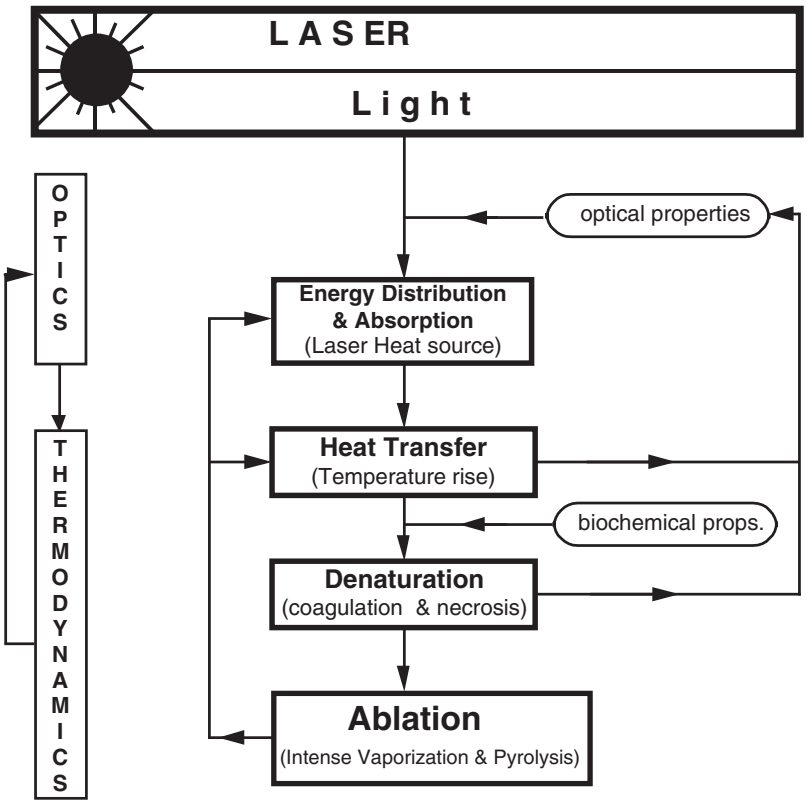

FIGURE 17.13 Flowchart of photothermochemical processes in thermal interaction of light with biological tissues.

Light including laser interaction with biological tissue is composed of a combination of optical and thermodynamical processes. An overview of these processes can be summarized as shown in Figure 17.13. Once light is irradiated on tissue, the photons penetrate into the tissue and, depending on the tissue optical properties such as scattering coefficient, absorption coefficient, and refractive index, the energy is distributed within the tissue. A portion of this energy is absorbed by the tissue and is converted into thermal energy, making the light act as a distributed heat source. This light-induced heat source in turn initiates a nonequilibrium process of heat transfer, manifesting itself by a temperature rise in tissue. The combined mechanisms of conduction, convection, and emissive radiation distribute the thermal energy in the tissue, resulting in a time- and space-dependent temperature distribution in the tissue. The temperature distribution depends on the thermal properties, conductivity, heat capacity, convective coefficients, and emissivity of the tissue.

As heat deposition and transfer continue, a certain threshold can be reached above which a process of irreversible thermal injury initiates. This process leads to coagulation of tissue caused by denaturation of enzymes and proteins and finally leads to necrosis of constituent cells. As a result of this thermochemical process of injury, properties of the tissue, especially

the optical properties, start to change. The change in properties in turn influences the process of energy absorption and distribution in the tissue.

The next stage in these processes is the onset of ablation. As the temperature continues to rise, a threshold temperature is reached, at which point, if the rate of heat deposition continues to exceed the rate at which the tissue can transport the energy, an intensive process of vaporization of the water content of the tissue combined with pyrolysis of tissue macromolecules initiates, which results in ablation or removal of tissue.

17.5.1 Temperature Field during Light/Laser Coagulation

In this section the governing equations are described for a thermodynamic analysis of light heating of biological tissues up to the onset of ablation. First, the heat conduction equation and typical boundary and initial conditions are described. Next the Arrhenius-Henriques model for quantitative analysis of irreversible thermal injury to biological tissue will be introduced.

Section 17.2 discussed how light energy is absorbed by a participating medium such as biological tissue. As light energy with a rate Q_L is absorbed by a material under irradiation, there is an immediate thermal energy flux traveling in different directions. This is caused by nonuniformity of Q_L in both the radial direction, due to beam profile, and the axial direction, due to absorption. The energy rate balance equation in the material can be found as follows.

Consider an infinitesimal element of the material under light/laser irradiation (Figure 17.14). The rate of thermal energy storage in the element, U, depends on the difference between incoming and outgoing thermal fluxes, the rate of light energy absorption, Q_L, and other energy rate interactions that are lumped together and labeled Q_o. The difference between influx and efflux is, in the limit, equal to the negative of the divergence of the thermal flux vector. So the energy rate balance can be written as

$$\partial U/\partial t = -\vec{\nabla} \cdot \vec{q} + Q_L + Q_o \tag{17.69}$$

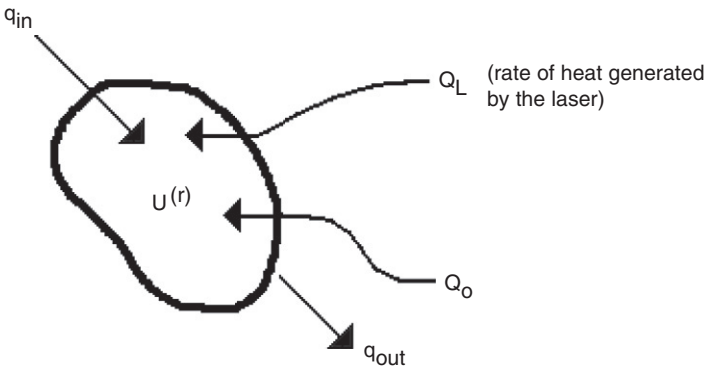

FIGURE 17.14 Thermal fluxes and energy in a control volume in the "material phase."

where $\vec{\nabla} \bullet \vec{q}$ is the change in thermal flux. The equation of state for thermal energy is

$$U = \rho C T \tag{17.70}$$

where T is an absolute temperature (K), ρ (kg/m^3) is the density, and C (joules/kg K) is the specific heat of the material.

At this point, as in the derivation of the photon phase, a phenomenological relation for the thermal flux is needed. The commonly used relation is known as Fourier's law, and it is written as

$$\vec{q} = -\kappa \vec{\nabla} T \tag{17.71}$$

where κ (W/m K) is the thermal conductivity of the material. Proceeding now by substituting Eqs. (17.71) and (17.70) into Eq. (17.69), the heat conduction equation is obtained:

$$\partial(\rho C T)/\partial t = \vec{\nabla} \cdot \kappa \vec{\nabla} T + Q_L + Q_o \tag{17.72}$$

This equation, solved with application of proper initial and boundary conditions, can, in theory, predict the temperature distribution in a material under laser irradiation.

In the case of biological tissue with other energy rates involved, Q_o can be written as

$$Q_o = Q_b + Q_m \tag{17.73}$$

where Q_b is the heat rate removed by blood perfusion, and Q_m is the rate of metabolic heat generation. These terms are not considered here. They are in general much smaller than the laser heat source term Q_L except when lower laser powers are used for longer times, as in hyperthermia treatments.

The material properties κ and ρC have been measured for many biological tissues, including human tissues. In general these properties may depend on temperature and water content, which could cause a nonlinear effect in Eq. (17.72). Another source of nonlinearity may be due to temperature dependence of the optical properties that, when present, has a more dominant role.

17.5.2 Thermal Coagulation and Necrosis: The Damage Model

The idea of quantifying the thermal denaturation process was first proposed in the 1940s. Using a single constituent kinetic rate model, this early work grossly incorporates the irreversible biochemical processes of coagulation, denaturation, and necrosis associated with thermal injury to biological tissue in terms of a single function. Defining an arbitrary nondimensional function, Ω, as an index for the severity of damage, the model assumes that the rate of change of this function follows an Arrhenius relation

$$\frac{d\Omega}{dt} = A \exp\left(-\frac{E}{RT}\right) \tag{17.74}$$

where R is the universal gas constant (cal/mole), T is the absolute temperature (K), and A (1/sec) and E (cal/mole) are constants to be determined experimentally. Total damage accumulated over a period t can be found by rearranging and integrating Eq. (17.74):

$$\Omega = A \int_0^t \exp\left(-\frac{E}{RT}\right) dt \tag{17.75}$$

The experimental constants A and E for pigskin were determined such that $\Omega = 1.0$ corresponded to complete transepidermal necrosis and $\Omega = 0.53$ indicated the minimum condition to obtain irreversible epidermal injury. The reported values are $A = 3.1 \times 10^{98}$ (1/sec), E = 150,000 (cal/mole). These values result in a threshold temperature of about 45°C. Different values for other tissues have been reported. For instance, for human arterial vessel walls, the values are $A = 4.1 \times 10^{44}$(1/sec), E = 74,000(cal/mole). For these values $\Omega = 1.0$ was defined as the threshold for histologically observed coagulation damage. It should be noted that the coagulation process—that is, collagen denaturation—is a different damage process than that seen in skin burns.

Once the heat conduction Eq. (17.72) is solved for the temperature field, the temperature history at every point in the tissue can be used in (17.75) to predict the accumulated damage at that point.

17.5.3 Photothermal Ablation

The temperature rise in a biological tissue under laser irradiation cannot continue indefinitely. A threshold temperature can be reached beyond which, if the rate of heat deposition by the light/laser continues to be higher than the rate heat can be transported by heat transfer mechanisms, intense vaporization of the water content of the tissue occurs. This results in creation of vacuoles—vacuolization—followed by pyrolysis at higher temperatures. The combined processes of intense vaporization—vacuolization—and pyrolysis of tissue macromolecule constituents is the "light/laser ablation process." This is the primary underlying mechanism for removal of tissue by laser surgery.

The large water content of most biological tissues suggests that the dominant part of the ablation process is the intense vaporization process. Apart from a short discussion of pyrolysis, intense vaporization is the main process of concern.

Following, a derivation is given for the ablation interface energy balance equation, which introduces the mathematical nonlinearity of the problem of ablation as a moving boundary problem. The section is concluded with a note on pyrolysis.

Ablation Interface Energy Balance Equation

The heat conduction equation alone cannot provide a mathematical model for determination of the dynamic behavior of the ablation front as a function of time. In fact, the motion of the ablation front influences the heat transfer process. An energy balance at the ablation front is needed in order to determine the motion of the front of ablation and its influence on the temperature field.

Consider a portion of a material under light irradiation with unit cross-sectional area and of thickness Δs, as shown in Figure 17.15, which is at the ablation threshold temperature

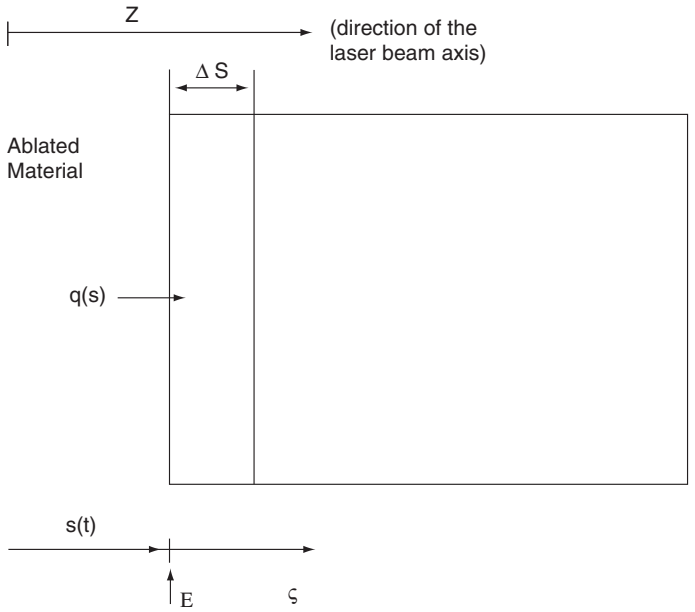

FIGURE 17.15 Ablation interface energy balance which is depicted as the amount of energy required to ablate a portion Δs of the tissue.

and is to be vaporized in the next interval of time Δt. Using Fourier's law for heat flux, Eq. (17.71), and after mathematical manipulations, the following equation for energy balance at the ablation interface can be derived

$$\kappa \frac{\partial T\,(s,\,t)}{\partial z} = \rho f_L L \frac{ds}{dt} \tag{17.76}$$

where f_L is the water fraction parameter. Nonlinearity inherent in the problem can be realized from this equation in that it couples the temperature gradient at the ablation interface to the rate of change of the front position, which is not known a priori. The solution requires an iteration procedure that requires the solution of the heat conduction equation simultaneously with the ablation front equation, with application of proper boundary and initial conditions.

Equation (17.76) is essential in providing information on the dynamics and thermodynamics of ablation. When solved simultaneously with the heat conduction equation and with the application of proper boundary and initial conditions, this equation provides the information on the position and velocity of the front of ablation. Furthermore, an important observation can be readily made about the temperature profile within the tissue, as discussed following.

Note that on the right-hand side of Eq. (17.76), ds/dt must be positive for the ablation process to proceed. This means that on the left-hand side, the temperature, $\partial T/\partial z$ must be positive. Consequently, the subsurface temperature must be higher than the surface temperature. That is, subsurface tissue must be superheated to temperatures higher than the

surface ablation temperature so thermal energy can be provided to the surface for the ablation process to proceed. This is in accordance with one of the corollaries of the second law of thermodynamics, stating that heat can be transported only from hotter points to colder points. In fact, the higher than ablation threshold temperature puts the subsurface tissue in a "metastable" equilibrium condition, which may be perturbed by internal tissue conditions and result in nucleation and vaporization initiating subsurface and manifesting itself by an "explosion" and mechanical tearing of the tissue surface. It should be noted at this point that initiation of the ablation process involves nonequilibrium nucleation processes that are not considered by the present approach.

17.5.4 Analytical Solution of Light Heating in a Purely Absorbing Medium

The governing equations for light irradiation with ablation were described in Section 17.5.3. Here, the governing equations will be repeated for a one-dimensional, semi-infinite, and purely absorbing medium. The governing equation for the preablation heating stage can be written as

$$\frac{\partial \rho c T}{\partial t} = \frac{\partial^2 T}{\partial z^2} + \mu_a I e^{-\mu_a z} \tag{17.77}$$

where μ_a is the absorption coefficient. This equation is valid up to the onset of ablation, which is assumed to occur when the surface temperature reaches the ablation threshold temperature, T_{ab}. The details of the analysis of ablation are beyond the scope of this chapter and will not be considered.

In the late 1970s, a nondimensionalization of the heat conduction equation for an axisymmetric three-dimensional case of preablation laser heating of tissue by a Gaussian beam in an absorbing medium was solved. The following relations will transform the governing equations into a dimensionless moving frame:

$$\theta = \frac{T - T_0}{T_{ab} - T_0} \qquad \xi = (I_0 c/kL)\, z \qquad \tau = (I_0 c/kL)(I_0/\rho L)t \tag{17.78}$$

The variables introduced are, respectively, dimensionless temperature θ, dimensionless coordinate ξ in the moving frame with origin at the ablation front, and dimensionless time τ. A dimensionless absorption parameter, B, and a dimensionless heating parameter λ are also defined as

$$\begin{aligned} B &= (kL/I_0 c)\alpha \\ \lambda &= c(T_{ab} - T_0)/L \end{aligned} \tag{17.79}$$

Analytical solutions of the nondimensional form of the governing equations can be found by Laplace transformation of the space variable ξ. The solution is as follows:

$$\theta(\xi, \tau) = \frac{1}{B\lambda}\left\{ 2B\sqrt{\tau}\ \text{ierfc}\left[\frac{\xi}{2\sqrt{\tau}}\right] - e^{-B\xi} + \frac{1}{2}e^{B^2\tau}\left(e^{-B\xi}\ \text{erfc}\left[B\sqrt{\tau} - \frac{\xi}{2\sqrt{\tau}}\right] + e^{B\xi}\ \text{erfc}\left[B\sqrt{\tau} + \frac{\xi}{2\sqrt{\tau}}\right]\right)\right\} \tag{17.80}$$

This equation describes the temperature field as a function of the dimensionless space variable ξ and dimensionless time τ and is valid up to the onset of ablation when $\theta = 1$. The symbol ierfc indicates the integral of the function erfc, $\text{ierfc}(z) = \int_z^\infty \text{erfc}(t)dt$. This equation can be implemented with relative ease using modern user-friendly computer tools such as MATLAB™ or Mathematica™. An example of the graph of this solution, which is the progression in time of the temperature profile as function of depth, is shown in Figure 17.16.

By letting $\theta = 1$ (i.e., $T = T_{ab}$) at $\xi = 0$ in Eq. (17.78), the following transcendental algebraic equation is obtained, which can be solved numerically for the time for the onset of ablation τ_{ab}:

$$B\lambda = \frac{2}{\sqrt{\pi}} B\sqrt{\tau_{ab}} + e^{B^2\tau_{ab}}\text{erfc}[B\sqrt{\tau_{ab}}] - 1 \tag{17.81}$$

Note that for large values of $B\ \lambda$, the behavior is almost linear with a slope of $\frac{2}{\sqrt{\pi}}$.

The present analysis did not consider the case of scattering tissue. An analytical solution for Q_L could be obtained using the diffusion approximation approach described in Section 17.2. However, implementation of that solution into Eq. (17.72) to solve analytically for temperature would be highly cumbersome at best. Therefore, a solution of temperature field would normally require a numerical approach, such as the finite difference or the finite element method.

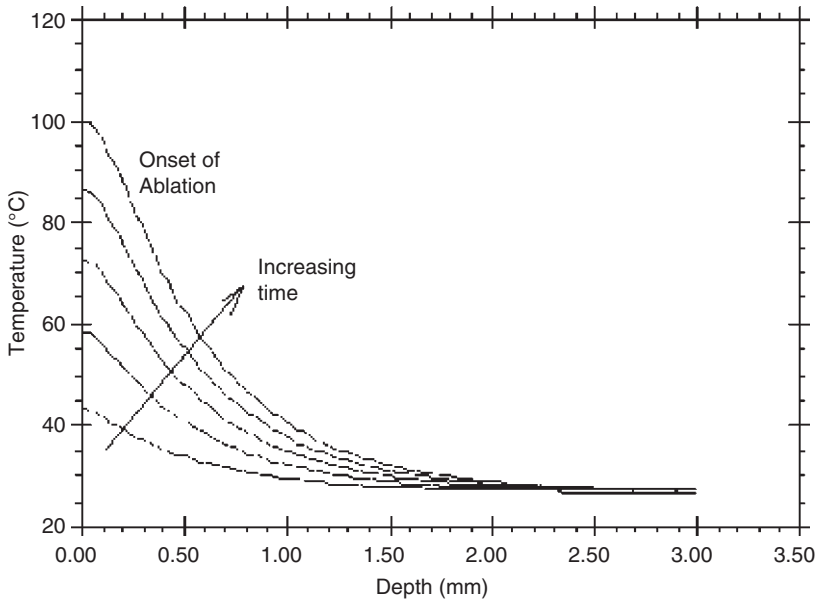

FIGURE 17.16 Nondimensional temperature as a function of nondimensional depth at various times prior to the onset of ablation.

17.5.5 Biochemical Damage Analysis

The Arrhenius model for prediction of damage was introduced previously. The damage function was defined in Section 17.5.2. For numerical computation, it is more convenient (due to large values of A and E) to rewrite the integrand of this function in an equivalent form so Eq. (17.83) becomes

$$\Omega(z,t) = \int_0^t \exp\left(\ln A - \frac{E}{RT(z,t)}\right) dt. \tag{17.82}$$

Two sets of values were used for A and E, one for pigskin and another for human vessel wall. The value of Ω(z,t) can be determined by replacing for T(z,t) from the analytical solution of the last section. The preablation solution should be used up to the onset of ablation, and after that, the ablation stage solution should be used.

The extent of damage or the position of the "damage front" at a given time t can be found by setting $\Omega = 1$ in Eq. (17.82) and solving for z. Alternatively, for every point z, Eq. (17.82) can be integrated by a controlled variable time-step procedure up to the time when $\Omega = 1$. The latter method was used to determine the position of the damage front as a function of time, and the difference in the value integrand at the upper and lower bounds of integration was monitored and used to change the time step. An example of such a calculation was done for a 5-watt laser pulse of 500 ms duration. The calculation was done using both values for A and E from both the pigskin and another for human vessel wall. The results, along with the position of the ablation front as a function of time (details of that are beyond the scope of this chapter), are shown in Figure 17.17.

The vertical line at about 0.0035 seconds indicates the onset of ablation, which helps to show that there had been biochemical damage in the tissue before the onset of ablation. After the onset of ablation, the difference between the damage front and ablation front is the actual extent of damage in the tissue intact. The important observation from this graph is the difference in prediction of the extent of damage using the two different sets of values for A and E. For the same irradiation conditions, thermal damage would propagate faster in skin than it would in vessel wall. This is expected, since the damage mechanisms for vessel wall and skin are different.

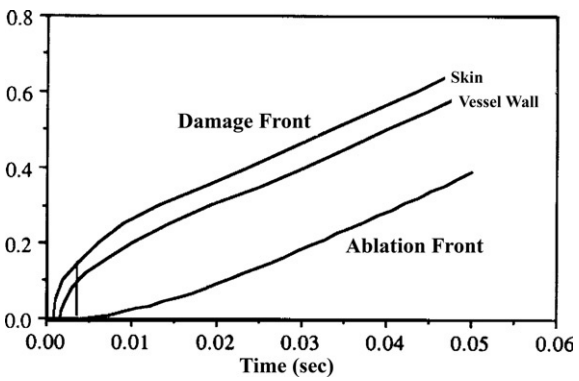

FIGURE 17.17 Damage front as a function of time.

EXAMPLE PROBLEM 17.9

Consider the skin subjected to a constant temperature heating T. For exposure durations t = 1 μs, t = 1 ms, t = 1s, t = 60s, and t = 30 minutes, find the critical temperature, T_c (in °C) required to achieve thermal damage, Ω = 1, during the exposure. Plot T_c versus exposure duration.

Solution

Given that the exposure durations are 1 μs, 1 ms, 1 s, 60 s, and 30 minutes, and R is the universal gas constant = 2 cal/gm-°C, then what is required for each case is for T_c (critical temperature at which point omega = 1) to be calculated.

Assumptions

Values of ln A and E are approximated to pig tissue values of 102.72 and 74,000, respectively.

Equation

$$\Omega(z,t) = \int_0^t \exp\left(\ln A - E/(RT(z,t))dt\right.$$

$$\therefore 1 = \int_0^t \exp\left(\ln A - E/(RT\_c)\right)dt \tag{ex1}$$

$$\therefore 1 = \int_0^t \exp\left(102.72 - 74000/(2{*}T\_c)\right)dt$$

$$\therefore 1 = \exp\left(102.72 - 74000/(2{*}T\_c)\right)\int_0^t dt \tag{ex2}$$

$$\therefore 1 = \exp\left(102.72 - 74000/(2{*}T\_c)\right)t \tag{ex3}$$

Solving Eq. (ex3) for all values of t, we can get T_c for those values. The tabulated values of t and T_c are as follows:

Exposure Time t (in s)	Critical Temperature T_c (in °C)
1 e-6	143.1548
1 e-3	113.153
1	87.2
60	74.56
1,800	72

17.5.6 Effect of Vaporization and Ablation Temperature

The coefficient f_L was introduced previously in relation to the heat of ablation as the water fraction parameter. Another nonvaporization phenomenon that can affect this coefficient is ejection of material due to subsurface nucleation. As was discussed, chunks of the material may be ejected without vaporization. Another factor that can affect the ablation

rate is the excess energy required for pyrolysis, which, as discussed before, manifests itself as a higher ablation threshold temperature.

Although the full solution of the ablation problem in this chapter was not considered, in order to understand how these phenomena affect the ablation rate, the steady-state ablation velocity may be used. This equation can be directly derived to be

$$v_{ss} = \frac{I}{\rho c \Delta T_{ab} + \rho f_L L}. \tag{17.83}$$

Fixing the values of I, ρ, c, and L, the effect of the parameters f_L and ΔT_{ab} on v_{ss} can be determined. In the following example, the physical properties of water are used, and I is chosen to be 267.8 W/cm2 so $v_{ss} = 1$mm/sec for $\Delta T_{ab} = 100$ °C and $f_L = 1$. Figure 17.18 shows the effect of ablation temperature on the ablation velocity for various values of f_L from 0.01 to 1.0. The general effect of an increase either in ablation temperature or in f_L is a decrease in ablation velocity as is also obvious from Eq. (17.83). Observe, however, that the larger the value of f_L, the less effect the ablation temperature has on the ablation velocity. For instance, whereas for $f_L = 0.1$ ablation, velocity drops from 4 mm/sec to 1.15 mm/sec over a temperature change from 100°C to 500°C for the same range, and for $f_L = 0.8$, the change is only from 1.20 mm/sec to 0.69 mm/sec. Therefore, if f_L should indicate the fraction of water in tissue, for example, a decrease in ablation rate should be of concern as a result of higher pyrolysis/ablation temperatures only for tissue with "low" water content (e.g., 30 percent or lower).

A cross section of families of curves in Figure 17.18 at $\Delta T_{ab} = 200$°C for more values of f_L is shown in Figure 17.19.

This figure shows that a change of f_L from 0 to 1 for $\Delta T_{ab} = 200$°C results in a change in the ablation velocity from 3.2 mm/sec to 0.86 mm/sec; that is, the ablation velocity can be

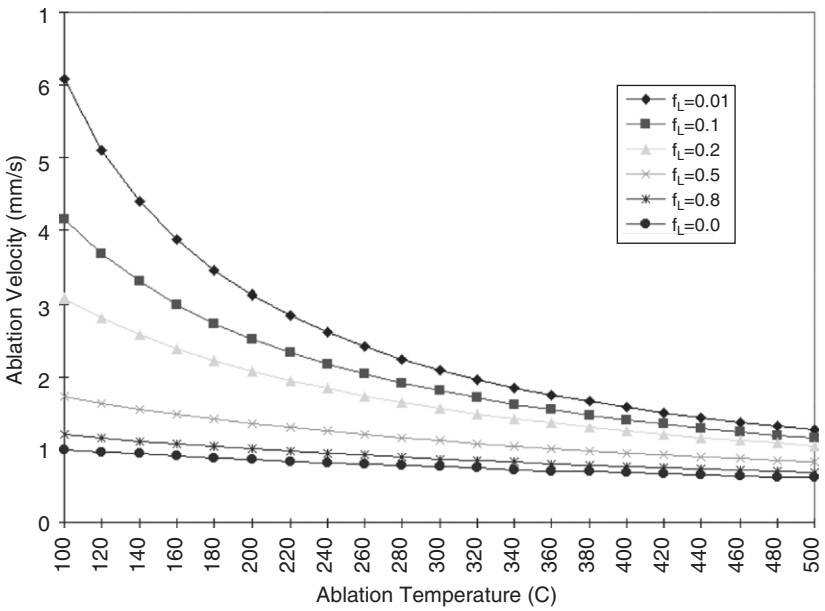

FIGURE 17.18 Effect of ablation temperature on ablation velocity for various water contents.

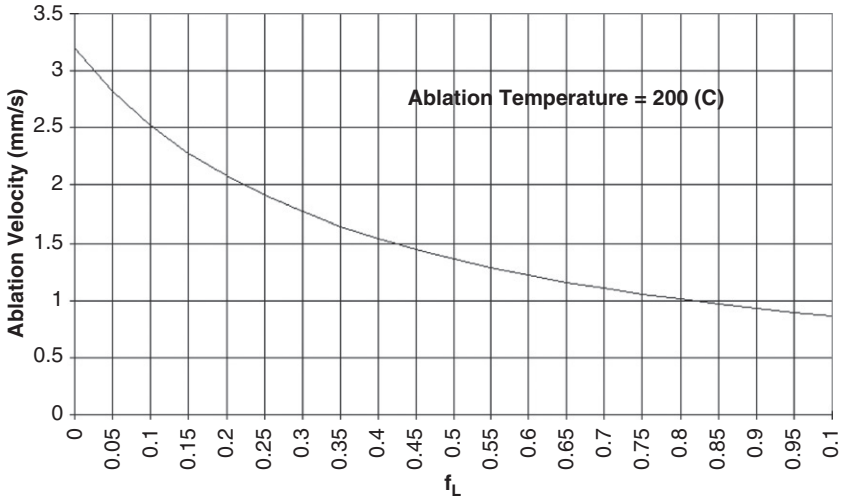

FIGURE 17.19 Effect of water content on ablation velocity.

over three times as large as its value for $f_L = 1.0$. The families of curves of Figure 17.18 are more closely packed at higher values of ablation temperature. This means that the effect of a change in f_L on the ablation velocity is less significant at higher ablation temperatures.

17.6 FIBER OPTICS AND WAVEGUIDES IN MEDICINE

Rigid tubes for the examination of body cavities had already been in use for thousands of years but in the 1800s illumination was added by means of a candle and a 45-degree mirror. The introduction in the early 1900s of multiple lenses to transmit images led to semiflexible tubes for insertion into the body. The use of fiber optic probes based on thin and transparent threads of glass dates back to the late 1920s but lay dormant for two decades until the idea was revived in the 1950s. The first medical instrument, a flexible fiber optic gastroscope, was developed and first used on patients in 1959. In the 1960s, the first lasers were developed, and in the early 1970s, there was a rapid development in the field of fiber optics for communications. All of these events have contributed to the modern fiber optic probes and endoscopes used today.

17.6.1 Principles of Fiber Optics and Waveguides

In Section 17.2.1, the interaction of light with a nonparticipating medium was described. In that section, light was described as rays, and the Fresnel equations for the interaction of the light rays at the boundaries of two media were derived. It was found that, depending on the index of refraction of two slab-types of materials and the angle of incident of the light, the amount of reflection and refraction could change. Although transmission of light through an optical fiber is a complex problem, the phenomenon

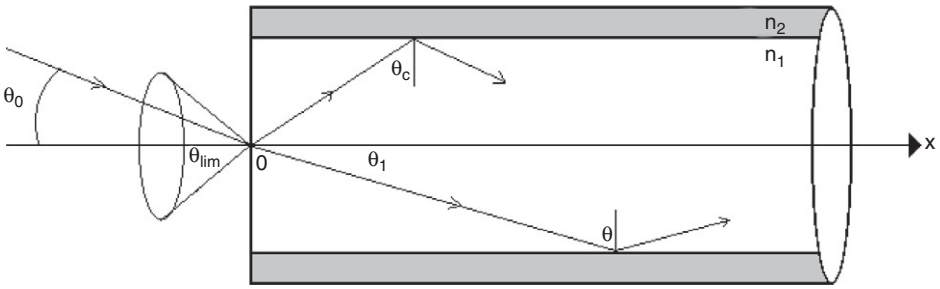

FIGURE 17.20 Basic model of an optical fiber with a cylindrical core with index of refraction (n_1) and cladding index (n_2), where ($n_2 < n_1$).

can be understood with a simple geometrical model. As shown in Figure 17.20, the fiber can be thought of as a long rod of transparent material in which the rod or core of the fiber has a higher index of refraction (n_1) than the surrounding cylindrical shell material or cladding (n_2). The propagation of the light occurs down the core because of the total internal reflection of the light from the core-cladding interface, which, from Snell's laws, occurs when the angle of reflection at this interface is greater than the critical angle. In order for the light to be internally reflected at the core-cladding interface, the light injected into the end of the fiber must be smaller than a cone with some limiting angle θ_o defined by

$$n_0 \sin(\theta_o) = (n_1^2 - n_2^2)^{1/2} = \text{NA} \tag{17.84}$$

where NA, which stands for "numerical aperture," is defined by this limiting value. In silica fibers the NA is generally between 0.2 and 0.4. As can be depicted in Eq. (17.84), increasing the difference in the index of refraction of the core and the cladding will increase the NA and also the acceptance angle. A large NA and acceptance angle produce a large number of rays with different reflection angles or, rather, different transmission modes. A different zigzag of the beam path is thus made for each mode. For a small core diameter, a single mode propagation can be generated in a fiber.

There are many different kinds of optical fibers that have been created with different structure, geometry, and materials, depending on the ultimate application. For instance, the tips of the fibers can be changed to produce side-firing beams for therapeutic applications such as coagulation of prostate tissue. The fiber tips can also be tapered for pinpoint application of the light beam or made as a diffuse tip for broad uniform application of the light. In general, optical fibers have been classified in terms of the refractive index profile of the core and whether there are single modes or multimodes propagating in the fiber. For instance, as shown in Figure 17.21, if the fiber core has a uniform or constant refractive index, it is called a step-index fiber; if it has a nonuniform, typically parabolic refractive index that decreases from the center to the cladding interface, it is known as a graded-index fiber; and if the fiber core is small with a low NA, only a single mode will propagate. The graded index fibers have been shown to reduce the modal dispersion by a factor of 100 times and increase the bandwidth over a comparably sized step-index fiber. These general classifications apply to most fibers, but special fiber geometries are often required, as

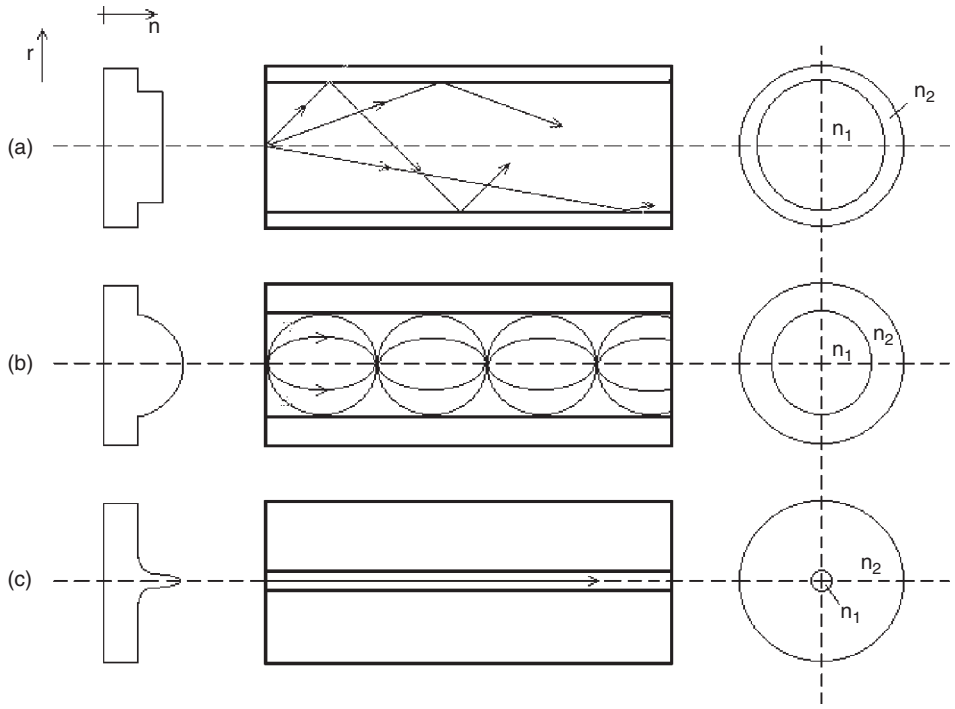

FIGURE 17.21 Typical geometry of the main types of optical fibers including a (a) step index, (b) graded index, and (c) single mode fiber.

discussed following, for endoscopic coherent fiber bundle fiber imaging, single fibers or noncoherent bundles for sensing and diagnostics, and optical fibers made for high-powered therapeutic applications.

In terms of the fiber material, three areas must be considered: the wavelength required, the power, and the biocompatibility. For therapeutic applications the amount of power, both for continuous lasers and pulsed lasers, needs to be considered. In particular, any impurities in the fiber may absorb the light and either decrease the amount of light reaching the probe for sensing or, for therapeutic applications, heat the fiber, which can then cause fiber damage. The fiber itself may also cause a pulsed laser to be broadened in time due to dispersion. In addition, besides impurities, the fiber material itself may work well for one wavelength and not work at all for others. For instance, the standard silica or glass fibers transmit well in the visible wavelength range, but beyond 2.0 micrometers these fibers absorb the light and thus cannot be used for infrared light transmission. Other fibers such as germanium, sapphire, barium fluoride, calcogenide, or hollow waveguide (i.e., gold coated) can be used for these wavelengths, but these fibers, in addition to impurities, may have problems for use in the body such as being too stiff, being hydroscopic (dissolves in water), or being toxic. Thus, the biocompatibility is a function of the material in that it needs to not be toxic to the patient and be able to function in the body without dissolving or breaking off.

17.6.2 Coherent Bundles for Imaging

Optical fibers can be bundled together in an aligned fashion such that the orders of the fibers at both ends are identical. Such a fiber bundle is called a coherent bundle or an ordered bundle. Note that the coherence here means the correlation between the spatial positions of the fibers at both ends and has nothing to do with the light coherence. The important property of coherent bundles is their capability to transmit images through a flexible channel. If an image is projected onto one end of a bundle, a replicate of the image is produced at the other end. Coherent bundles of optical fibers are the key components in endoscopes.

In endoscopic applications, an internal organ is imaged and viewed outside the body in a minimally invasive fashion. An incoherent (nonordered) bundle of optical fibers is used to illuminate the portion to be imaged inside the human body. A coherent (ordered) bundle of optical fibers is used to transmit an image of the target portion. A white light source is usually used for the illumination so an accurate color image of the tissue can be obtained.

The quality of image transmission is mainly determined by two factors: light collection and image resolution. The collection power of each individual optical fiber is limited by the diameter of its core and the numerical aperture (NA). A large NA and core diameter allow a good transmission of light from the illuminated object to the eye of the physician. The image resolution indicates how fine details can be seen and is limited by the core diameter, d, of the cores of the individual fibers. The resolution, in number of discernible lines per millimeter, is approximately $d/2$. The smaller the core diameter, the better the image resolution. Due to the limited resolution, a straight line in an object may appear zigzagged in the image.

Cladding of each individual optical fiber is required to minimize or avoid crosstalking among the fibers. Unclad fibers were used in early endoscopes and had poor imaging quality. Light in unclad fibers may leak from the core and cross into other fibers. The crosstalk causes an overlay of various portions of an image during transmission and results in a blurred image.

The requirements of high light collection and good image resolution have conflicts. A large core diameter allows good light transmission but gives poor resolution. A thick cladding layer avoids crosstalk but limits light collection and image resolution. A tradeoff has to be made. In practice, the core diameter is usually 10–20 μm, and the cladding thickness is of the order of 1.5–2.5 μm.

Several other factors may deteriorate the image obtained with a coherent bundle. Some stray light may transmit through the cladding layers into the cores. The stray light would add an undesirable background that reduces the image contrast. Defective fibers in a coherent bundle would cause a serious problem. If a defective fiber does not transmit any light, a static dark spot appears in the image. If the ordering of the fibers is not identical at both ends, image distortion will degrade the images.

Lenses may be added at both ends of an imaging coherent bundle to adjust the magnification. Although the distance between the objective lens and the fiber bundle can be adjusted in principle to adjust the focusing of the coherent bundle, a fixed focus with a large depth of focus is often used for simplicity. A digital image acquisition board can be used to capture the image in a computer for display, or a VCR can be used to record the images in real time while the images are displayed on a monitor.

Endoscopes may be specially built for imaging of various organs. The following is a list of commonly used endoscopes: angioscopes for veins and arteries, arthroscopes (or orthoscopes) for the joints, bronchoscopes for the bronchial tubes, choledoschoscopes for the bile duct, colonoscopes for the colon, colposcopes for the vagina, cystoscopes for the bladder, esophagoscopes for the esophagus, gastroscopes for the stomach and intestines, laparoscopes for the peritoneum, laryngoscopes for the larynx, and ventriculoscopes for the ventricles in the brain.

17.6.3 Diagnostic and Sensing Fiber Probes

In terms of sensors for minimally invasive measurements into the body, the use of fiber optic probes began to thrive beginning in the 1980s. To understand the potential capability of these probes, a sensor is first defined along with some of the requirements for a good sensor. A sensor is a device that transforms an input parameter or measurand into another parameter known as the signal. For instance, a displacement membrane on the tip of a fiber probe could transform a pressure signal into a light intensity change that is then depicted as a change in voltage from a light detector. The requirements for any good sensor are specificity or the ability to pick out one parameter without interference from the other parameters, sensitivity or the capability to measure small changes in a given measurand, accuracy or closeness to the true measurement, and low cost. As with most sensors, fiber optics have to trade off these parameters to within some limit. For example, you may be able to get 95 percent accuracy at a reasonable cost, but obtaining 99 percent accuracy might require a huge increase in cost, so one must trade off what might be clinically acceptable given the cost. Fiber optic probes offer the potential to meet the preceding sensor requirements, as well as provide for miniaturization; good biocompatibility for the visible and near-infrared wavelengths; speed, since light is used; and safety, since no electrical connections to the body are required.

All fiber optic probes transmit light into the body, and the light, directly or indirectly, interacts with the biological parameter of interest, be it a biological fluid, tissue, pressure, or body temperature. The interaction causes a change in the light beam or beams that travel back to the detection system. The returning signal can be physically separated from the input signal in a separate fiber or fibers, or it can be separated if the output beam is at a separate wavelength from the input beam, as is the case for fluorescence probes. Fiber optic sensors can be used for each of the preceding chemically and physically based measurements described in Sections 17.3 and 17.4. However, rather than try to discuss each fiber optic probe for each application, the rest of this section will be focused on separating the fiber probes into two classes: indirect and direct fiber optic sensors. Direct fiber optic sensors are defined as those probes in which the light interacts directly with the sample. For instance, absorption measurements can theoretically be made to determine such things as blood oxygenation or to quantify blood analytes with either two side firing fiber optic probes separated at a fixed distance, as shown in Figure 17.22a, or an evanscent wave fiber optic, which has the cladding stripped off so some of the light travelling down the core travels out of the fiber, interacts with the sample, and then returns to the fiber core, as shown in Figure 17.22b.

In Figure 17.22c, a fiber optic bundle is depicted that could be used to transmit and receive light to and from tissue to distinguish between normal and cancerous or

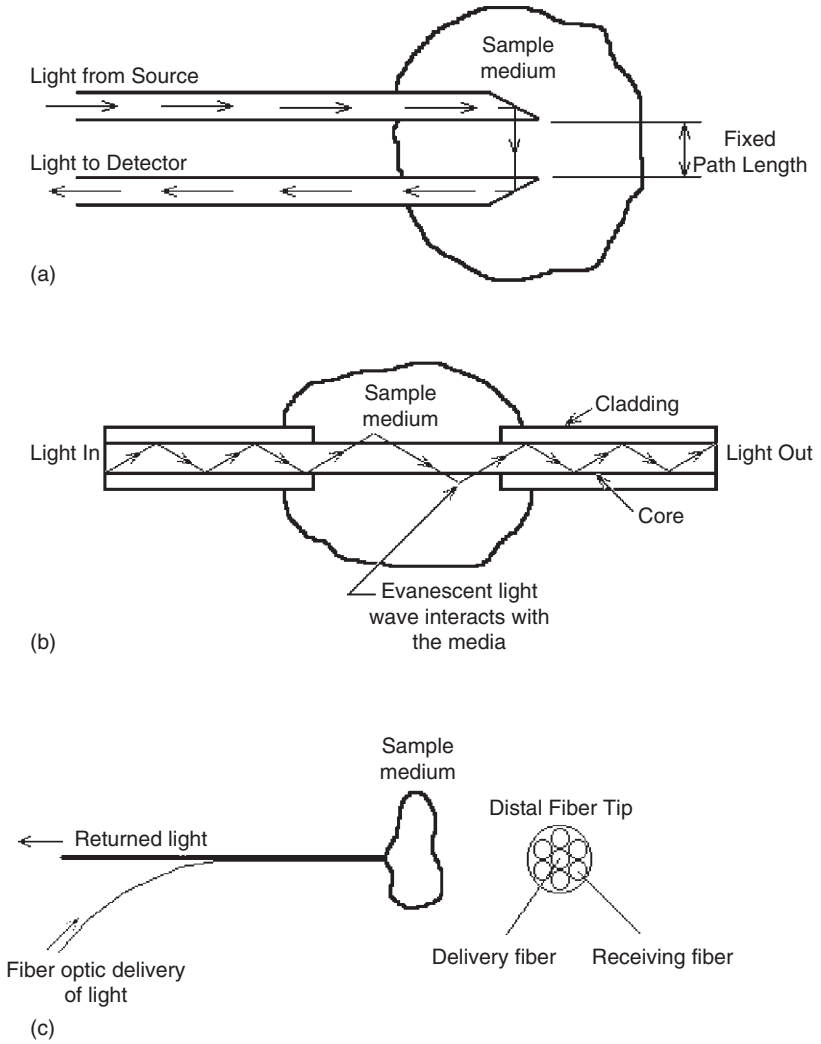

FIGURE 17.22 Direct fiber optic probe designs including (a) absorption probe using two side firing fibers, (b) an evanescent wave probe in which the light transmits from the core to the sample and back into the core, and (c) a multifiber design for use in distinguishing normal from cancerous tissue by directly measuring autofluorescence or Raman spectra.

precancerous lesions using direct measurement of tissue autofluorescence or Raman spectrum. Interferometers, such as the Fabrey-Perot type described in Section 17.3.4, have been designed using partially reflecting mirrors built into a fiber optic, and any physical change imparted on the fiber, such as that due to fluctuations in body temperature or pressure, can be directly measured by the fiber in the form of a change in the interference pattern of the light. Finally, the fiber optic probe for measurement of tissue optical properties, described in Section 17.2.4, is another example of a direct probe that measures reflections from the

sample. It should be noted that each of these descriptions is somewhat oversimplified in that a great deal of design needs to be done to gain the specificity, accuracy, and sensitivity required to measure these various low-level parameters in the noisy environment of the body. For indirect fiber optic measurements, a miniaturized transducer (sometimes referred to as on optode) is attached to the distal end of the fiber so the light interacts with this transducer and the transducer interacts with the sample. A displacement optode such as that shown in Figure 17.23a can be used to monitor pressure or temperature changes by simply causing less light to be specularly reflected into the fiber as the tip is moved. In addition, fluorescent chemistry can be placed within a membrane on the distal tip of the fiber, as shown in Figure 17.23b, in which the amount of fluorescent light produced is a measure

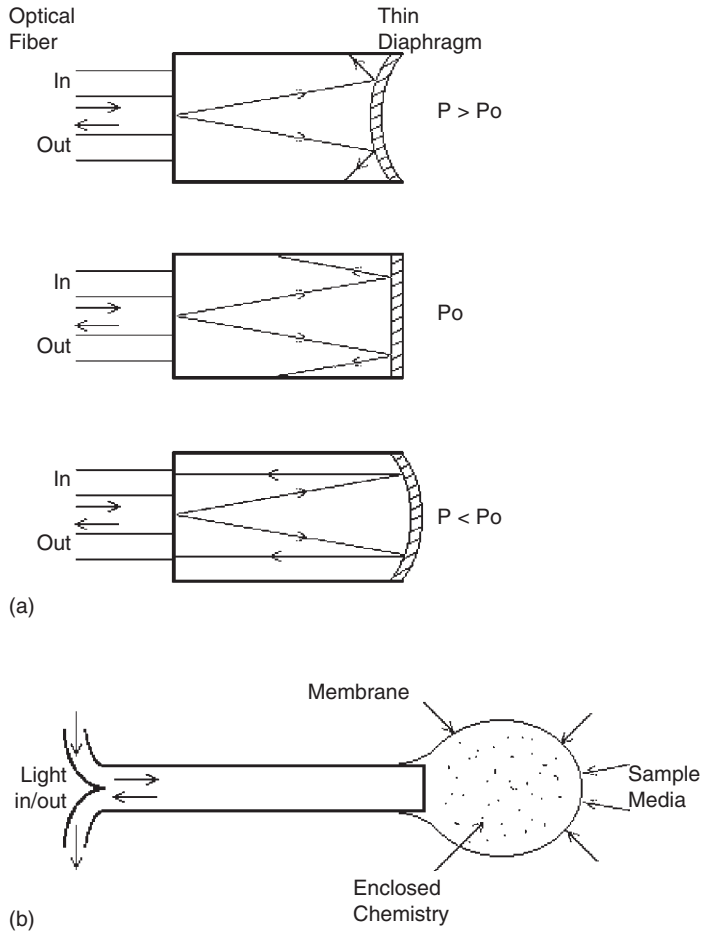

FIGURE 17.23 Indirect fiber optic probe designs including (a) a thin reflectance diaphragm for pressure or temperature measurements, and (b) an optode with some chemistry enclosed within a membrane at the distal tip of the fiber, which can be used, for instance, to determine a particular analyte concentration using fluorescent chemistry specific to the analyte of interest.

of the concentration of a particular blood analyte. These indirect methods of measurement are also simplified, and the actual final design to obtain an accurate and sensitive signal can be quite complicated. Overall, the indirect fiber optic measurements typically have higher specificity over direct measurement approaches but at the expense of requiring a more complicated probe.

17.7 BIOMEDICAL OPTICAL IMAGING

Medical imaging has revolutionized the practice of medicine in the past century. Physicians are empowered to "see" through the human body for abnormalities noninvasively and to make diagnostic decisions rapidly, which has impacted the therapeutic outcomes of the detected diseases.

Medical imaging dates back to 1895 when x-rays were discovered serendipitously by German physicist W. C. Roentgen, who received the first Nobel Prize in physics in 1901 for this important work. Human anatomy can be easily imaged by simple x-ray projections, such as chest x-rays, that are still used today. Contemporary medical imaging began with the invention of computerized tomography (CT) in the 1970s. G. N. Hounsfield in England produced the first computer reconstructed images experimentally, and A. M. Cormack in the United States laid the theoretical foundation. Both of them were awarded the Nobel Prize in medicine in 1979. The essence of CT is that if an object is viewed from a number of different angles, then a cross-sectional image of it can be computed—that is, "reconstructed."

The advent of CT has inspired other new tomographic and even 3D imaging techniques. The application of reconstruction to conventional nuclear medicine imaging led to positron emission tomography (PET) and single photon emission computed tomography (SPECT). A similar application to the technique of nuclear magnetic resonance led to magnetic resonance imaging (MRI).

Different imaging modalities are used to detect different aspects of biological tissues through a variety of contrast mechanisms. X-ray imaging senses primarily electron density and atomic number. In MRI, proton density and its associated relaxation properties are detected. Ultrasonography images use acoustic impedance mismatches for contrast. In nuclear imaging, nuclear radiation emitted from the body is detected after introducing a radiopharmaceutical inside the body to tag a specific biochemical function.

The advantages and disadvantages of different imaging modalities may be illustrated using breast cancer detection. Breast cancer is the most common malignant neoplasm and the leading cause of cancer deaths in women in the United States. A means for prevention of breast cancer has not been found, and early detection and treatment are the best solutions to improving the cure rate. At present, x-ray mammography and ultrasonography are clinically used for breast cancer detection. Mammography is currently the only reliable means of detecting nonpalpable breast cancers. As a supplementary tool, ultrasound is used to evaluate the internal matrix of circumscribed masses found using mammography or of palpable masses that are obscured by radiographically dense parenchyma using mammography. However, x-ray mammography is ionizing radiation, and imaging of radiographically dense breasts is difficult. Ultrasonography cannot detect many of the nonpalpable cancers that are not visible on mammograms of good quality.

Several other techniques are under investigation for breast cancer imaging. Magnetic resonance imaging (MRI) offers great promise for imaging of the radiographically dense breast. Breast MRI is superior to mammography in differentiating solid from cystic lesions and is equivalent to mammography in providing information regarding different parenchymal patterns. Injection of intravenous contrast material with MRI increases cancer detectability even though breast cancer and glandular tissues have similar magnetic resonance tissue characteristics. However, breast MRI is expensive, has inferior spatial resolution to mammography, and cannot image microcalcifications. Breast CT has been investigated for the differentiation of benign from malignant solid masses. Because breast CT involves the use of intravenous injection of iodinated contrast material and is expensive, it is not suited for routine breast cancer screening.

17.7.1 Optical Tomographic Imaging

Nonionizing optical tomography is a new and active research field, although projection light imaging was investigated as early as 1929. The optical properties of normal and diseased tissues are usually different despite the large variation of values in optical properties of the normal tissues alone. Therefore, it is possible to detect some breast cancers based on measurements of optical properties.

The optical difference is not surprising because cancerous tissues manifest significant architectural changes at the cellular and subcellular levels, and the cellular components that cause elastic scattering have dimensions typically on the order of visible to near-IR wavelengths. Some tumors are associated with vascularization, where blood causes increased light absorption. The use of optical contrast agents may also be exploited to enhance the optical contrast between normal and abnormal tissues. Because the optical information is determined by the molecular conformations of biological tissues, optical imaging is expected to provide sensitive signatures for early cancer detection and monitoring.

Because tissues are optically turbid media that are highly scattering, light is quickly diffused inside tissues as a result of frequent scattering. The strong scattering has made optical detection of biological tissues challenging. A typical scattering coefficient for visible light in biological tissues is 100 cm^{-1} in comparison with 0.2 cm^{-1} for x-rays used in medical diagnostics. Light transmitted through tissues is classified into three categories: ballistic light, quasi-ballistic light, and diffuse light. Ballistic light experiences no scattering by tissue and thus travels straight through the tissue. Ballistic light carries direct imaging information just as x-ray radiation does. Quasi-ballistic light experiences minimal scattering and carries some imaging information. Multiply-scattered diffuse light carries little direct imaging information and overshadows ballistic or quasi-ballistic light in thick biological tissue.

One of the techniques used for optical tomography is called "early-photon imaging." If diffuse light is rejected, and ballistic or quasi-ballistic light is collected, buried objects can be detected much like x-ray projection. This technique uses a short-pulse laser ($<$1 ps pulse width) to illuminate the tissue. Only the initial portion of transmitted light is allowed to pass to a light detector, and the late-arriving light is gated off by a fast optical gate. Because the ballistic or quasi-ballistic photons travel along the shortest path length, they arrive at the detector sooner than diffuse photons. If only ballistic light is detected, the technique is called ballistic imaging. It has been shown that ballistic imaging is feasible only for tissue

of thickness less than 1.4 mm or 42 mean free paths. Most ballistic imaging techniques reported in the literature have achieved approximately 30 mfp. Therefore, this approach is suitable for thin tissue samples but suffers loss of signal and resolution for thick tissues as a result of the strong scattering of light by the tissue.

EXAMPLE PROBLEM 17.10

Calculate the decay of ballistic light after penetrating a biological tissue 30 mean free paths thick. If the scattering coefficient of the tissue is 100 cm^{-1}, calculate the corresponding thickness in cm.

Solution

Based on Beer's law, the decay is $\exp(-30) = 9.4 \times 10^{-14}$. The thickness is $30/100 = 0.3$ cm.

For tissue of clinically useful thickness (5 to 10 cm), scattered light must be used to image breast cancers. It has been shown that for a 5-cm-thick breast tissue with an assumed absorption coefficient of 0.1 cm^{-1}, and reduced scattering coefficient of 10 cm^{-1}, the detector must collect transmitted light that has experienced at least 1,100 scattering events in the tissue to yield enough signal. Therefore, ballistic light or even quasi-ballistic light does not exist for practical purposes. However, if a 10 mW visible or near-infrared laser is incident on one side of the 5-cm-thick breast tissue, it has been estimated, using diffusion theory, that the diffuse transmittance is on the order of 10 nW/cm^2 or 1,010 photons/(s cm^2), which is detectable using a photomultiplier tube. Similarly, the diffuse transmittance through a 10-cm-thick breast tissue would be on the order of 1 pW/cm^2 or 106 photons/(s cm^2). The significant transmission of light is due to the low absorption coefficient despite the high scattering coefficient.

Imaging resolution of pure laser imaging degrades with increased tissue thickness. The temporal profiles of the scattered light may be detected using a streak camera. The early portion of the profiles was integrated to construct the images of buried objects in a turbid medium. This time-domain technique requires expensive short-pulse lasers and fast light detectors.

Optical-coherence tomography (OCT) has emerged as a useful clinical tool. This technique is based on the Michelson interferometer (see Figure 17.9) with a short-coherence length light source. One arm of the interferometer leads to the sample of interest, and the other leads to a reference mirror. The reflected optical beams are detected at the photodetector. The two beams interfere only when the sample and the reference path lengths are equal to within the source coherence length. Heterodyne detection is performed by taking advantage of the direct Doppler frequency shift that results from the uniform high-speed scan of the reference path length. Recording the interference signal magnitude as a function of the reference mirror position profiles the reflectance of the sample, which produces an image similar to an ultrasonic A scan. OCT has achieved less than 10 μm resolution with a penetration depth of approximately 1 mm.

OCT was extended to image blood flow in superficial vessels based on Doppler shift. The blood flow causes a Doppler shift on the frequency of the light. Frequency analysis with Fourier transformation of the optical interference signal yields the Doppler shift, which is used to calculate the velocity of the blood flow.

A technique for optical imaging of thick tissue is the frequency-domain technique, which is based on photon-density waves. The governing equation of photon-density waves is the diffusion equation

$$\partial\Phi(r,t)/c\partial t + \mu_a\Phi(r,t) - D\nabla^2\Phi(r,t) = S(r,t) \tag{17.85}$$

where $\Phi(\boldsymbol{r},t)$ is the light fluence rate at point $\boldsymbol{r}$ and time t [W/cm^2], c is the speed of light in the medium [cm/s], μ_a is the absorption coefficient [cm^{-1}], and $S(\boldsymbol{r},t)$ is the source intensity [W/cm^{-3}]. The frequency-domain imaging technique requires the use of inverse algorithms for image reconstruction. Amplitude-modulated (at approximately 100 MHz) laser light is used to illuminate the tissue at multiple sites. At each illumination site, an optical detector measures the amplitude and phase of diffuse light at multiple locations around the tissue. The measured diffuse light can be estimated by the diffusion equation, Eq. (17.85), if the optical properties of the tissue sample are known. Conversely, the optical properties can be calculated by use of the measured diffuse light, which is the image reconstruction. A sample reconstructed image is shown in Figure 17.24, which was based on a theoretically generated data set of diffuse light.

17.7.2 Hybrid Optical Imaging

Several emerging imaging techniques are being developed by combining relatively transparent acoustic energy with strongly scattering light, which is called hybrid optical imaging. Ultrasound-modulated optical tomography, photoacoustic tomography, and sonoluminescence are briefly discussed.

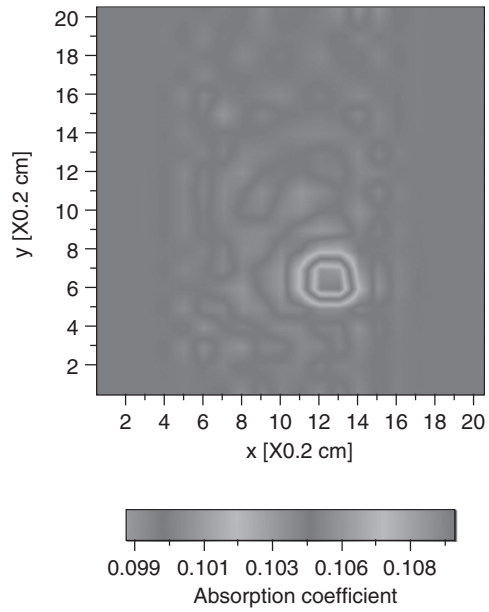

FIGURE 17.24 Sample reconstructed image using photon-density waves. A simulated tumor with elevated absorption coefficient is visible in the lower right quadrant.

In ultrasound-modulated optical tomography, an ultrasonic wave is focused into a scattering medium to modulate the laser light passing through the medium containing buried objects. The modulated laser light collected by a photodetector is related to the local mechanical and optical properties in the zone of ultrasonic modulation. If the buried objects have optical properties that are different from those of the background scattering medium, an image can be obtained by raster-scanning the device.

In photoacoustic tomography, a short-pulse light beam illuminates the scattering medium. The light is diffused in the medium and partially absorbed. If there is a strong optical absorber such as a tumor in the middle of the medium, more light will be absorbed by this optical absorber than by its neighboring background. The absorbed optical energy is converted into heat. Due to thermal elastic expansion, an acoustic wave is generated. Stronger heat generation will produce a stronger acoustic wave. Therefore, a strong optical absorber emanates a strong acoustic wave. If multiple acoustic transducers are used to measure the acoustic signal around the medium, the absorber can be located based on the temporal distribution of the acoustic signals and thus produce an image of the medium. Functional and molecular imaging has been achieved.

The inverse of photoacoustic tomography is sonoluminescent tomography (SLT). The ultrasonic generation of light known as sonoluminescence (SL) was first reported in 1934, which was multiple-bubble sonoluminescence (MBSL). SL has attracted an extraordinary amount of attention in this decade, since single-bubble sonoluminescence (SBSL) was reported in 1990. Although the full explanation of SL is still in development, it is well known that light is emitted when tiny bubbles driven by ultrasound collapse. The bubbles start out with a radius of several microns and expand to about 50 microns due to a decrease in acoustic pressure in the negative half of a sinusoidal period. After the sound wave reaches the positive half of the period, the situation rapidly changes. The resulting pressure difference leads to a rapid collapse of the bubbles accompanied by the emission of light. The flash time of SL has been measured to be in the tens of picoseconds. SBSL is so bright that it can be seen by the naked eye even in a lighted room, whereas MBSL is also visible in a darkened room. Researchers have envisioned possible applications of SL in sonofusion, sonochemistry, and building ultrafast lasers using the ultrafast flash of light in SL.

SLT is an application of SL that has been developed for cross-sectional imaging of strongly scattering media noninvasively. Sonoluminescence, which is generated internally in the medium by exposure of the medium to external ultrasound, is used to produce images of a scattering medium by raster-scanning the medium. The spatial resolution is limited by the focal spot size of the ultrasound and can be improved by tightening the focus.

Optical imaging techniques may also measure the optical spectra of biological tissues noninvasively. Besides the absorption spectra that are usually measured for other materials, the scattering spectra may also be measured. The optical spectra may be used to quantify important physiological parameters such as the saturation of hemoglobin oxygen.

In summary, optical imaging and biomedical optics techniques in general have the advantages of (1) the use of nonionizing radiation, (2) the capability of measuring functional (physiological) parameters, (3) the potential high sensitivity to the pathologic state of biological tissues, and (4) low cost. However, biomedical optics is a challenging research field in its infancy, and as it grows, it will continue to require the participation of many diverse talented physicians, scientists, and engineers.

17.8 EXERCISES

1. (a) Name at least three reasons why it might be desirable to use optic or fiber optic sensors for biomedical applications. (b) Name three potential drawbacks to using optic or fiber optic biomedical sensors.
2. In one paragraph, or using bullets, explain the similarities and differences among polarization, luminescence, absorption, scatter, and Raman scattering of light.
3. Given an interface between clear tissue (i.e., water; $n_t = 1.33$) and glass ($n_g = 1.5$), compute the transmission angle for a beam incident in the water at 45°. If the transmitted beam is reversed so it impinges on the interface from the glass side, calculate what the transmitted angle will be through the tissue. Does this make sense? Explain.
4. Using MATLAB, or some other software, plot ($R_\perp = r_\perp{}^2$) and ($R_p = r_p{}^2$) as a function of the input angle θ_i for a glass ($n_i = 1.5$) and air ($n_t = 1.0$) interface. Explain what it means.
5. An Nd:YAG laser operating at 1,064 nm with a Gaussian beam is to be used for performing a port-wine stain treatment. Assume a heuristic model for light distribution in a homogeneous material such that $I(r,z) = I_o \exp(-\mu z) \exp(-2(r/\omega_b)^2)$, where $\mu = \mu_a + \mu'_s$, μ_a and μ'_s being the absorption and reduced scattering coefficients. For the following multilayer case at $r = 0$, give the expressions and graph intensity I and the rate of heat generation Q in the tissue by the laser, $I(r = 0,z)$ and $Q(r = 0,z)$. Assume $I_o = 1$. The absorption and scattering coefficients of each skin layer and blood vessel for this wavelength are given below. Discuss how selective photothermolysis of the blood layer is achieved.

	μ_a (cm^{-1})	μ'_s (cm^{-1})
Blood	20	20
Epidermis	0.1	10
Dermis	0.5	10

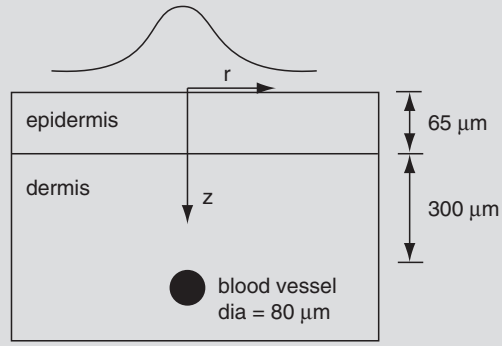

6. Consider a turbid biological tissue with an absorption coefficient of $\mu_a = 0.1\ \text{cm}^{-1}$. Using the diffusion approximation, graph on the same plane the logarithm of relative intensity versus radius for four different values of reduced scattering coefficient—$\mu'_s = 1$, 10, 50, and 100 cm^{-1}—r varying from 0.1 cm to 2 cm. Describe the results in terms of the effect of scattering on the intensity profile.
7. For liver tissue irradiated by the pulsed Ho:YAG laser, determine the exposure duration during which the equation for heat conduction may be ignored. Assume that the absorption coefficient at the Ho:YAG laser wavelength is 30 cm^{-1}, and assume the thermal diffusivity of the tissue is the same as that of water. If the threshold temperature of ablation is 150°C, determine the threshold fluence (J/cm^2) for ablation.

8. Given a Helium-Neon laser-based fiber optic Doppler probe at an angle of 60° with a blood vessel that registers a frequency shift of 63 KHz, what is the velocity of the blood? Is this a reasonable number from a physiologic point of view when compared to the average velocity in the major and minor blood vessels in the human body?
9. Assume you want to measure the thickness of a piece of tissue ($n_t = 1.33$) bounded by air ($n_a = 1.0$) using either the Michelson or Fabry-Perot interferometric approach. Your light source has a wavelength of 780 nm, and your instrument can count 20 fringes. The tissue is ablated (or cut) with a high-powered pulsed laser that removes roughly 2 micrometers of tissue per pulse. The maximum tissue thickness before it is all removed is 20 micrometers. (a) Calculate to see if each of the interferometer systems will have a long enough dynamic range, without moving the system, to be used with this piece of tissue. Explain your result. (b) Assume you want to use either of your interferometric systems as a feedback unit for the laser removal of tissue. What is the range in the number of fringes (m_{min} and m_{max}) for each of your systems in order to measure both the minimum slice thickness and the maximum tissue thickness? Explain.
10. In general, when is a Fabry-Perot interferometer preferred over a standard Michelson interferometer? Can you make a Fabry-Perot interferometer that performs worse than a Michelson interferometer? Explain.
11. For Raman spectroscopy, what are the Stokes and anti-Stokes bands? Which bands are typically used for sensing? What are the main challenges to overcome for Raman spectroscopy to be used for biomedical sensing?
12. Assume you want to measure glucose through the anterior chamber of the eye as a means of noninvasively quantifying blood glucose. Given that glucose has a specific rotation of 41.89 degrees/(dm g/ml) at a wavelength of 656 nm, and the anterior chamber of the eye has a path length of roughly 0.8 cm, calculate the concentration of glucose for a rotation of 15 millidegrees. Is this a reasonable value from a physiologic point of view? Would the patient be considered normal or diabetic? Explain your result.
13. In the near-infrared region of the optical spectrum between 600 and 1,100 nanometers, there are well-known absorbance peaks for oxygenated and deoxygenated hemoglobin. A big assumption can be made for the moment that in this region the dominant optical signal is due to absorption (which is not generally the case). Given that you propagate through a 2-centimeter sample of tissue, you need to calculate three parameters: the concentration of oxyhemoglobin, deoxyhemoglobin, and a background blood absorbance. At three wavelengths (758 nm, 798 nm, and 898 nm), you can measure the extinction coefficients for oxygenated (1.612, 2.072, and 2.763 $mM^{-1}\,cm^{-1}$) and deoxygenated (3.914, 2.072, and 2.072 $mM^{-1}\,cm^{-1}$) hemoglobin, respectively. The total absorption coefficients at these three wavelengths in the tissue can be measured using a time-resolved system as 0.293 cm^{-1}, 0.1704 cm^{-1}, and 0.1903 cm^{-1}, respectively. Calculate the oxygenated and deoxygenated hemoglobin levels given these parameters. Is this reasonable from a physiologic point of view? Explain.
14. Using the parameters of the equation for problem 7, give a graph of temperature versus time at $z = 0$, for t varying from 0 to 1 ms, using the analytical solution of the heat conduction

Continued

equation given in the chapter. On the same graph, plot the temperature, ignoring the effect of conduction, which assumes linear variation with time. Comment on your findings in relation to the diffusion time found in problem 7.

15. Consider skin tissue that is exposed to linear heating—for example, as in pulsed laser coagulation—such that $T = T_o + \text{mt}$, when T_o is the initial temperature (e.g., 37°C) and m is the rate of heating (e.g., 10^3 °C/s). Describe how you would find the critical temperature for thermal damage. Do you expect that to be lower or higher than the constant temperature case of the same exposure duration?

16. For the study of ablation onset time, plot A graph of $\text{B}\sqrt{\tau_{\text{ab}}}$ versus $\text{B}\lambda$. Measure the slope for "large" values of $B\ \lambda$; it should be $\frac{2}{\sqrt{\pi}}$. For absorption coefficient 100/cm and a laser intensity 1,000 W/cm^2, find the time for the onset of ablation using water thermal properties, assuming ablation initiates at 150°C.

17. In the visible optical region, tissue scattering dominates absorption. Assume that the scattering coefficient of a 5-cm-thick tissue is 100 cm^{-1} and the wavelength of light is 0.5 μm. In order to detect on average a single ballistic photon transmitted through the tissue, what is the energy in Joules that is required for the incident light? Compare the energy of the incident light with the rest energy of the earth using Einstein's mass-energy equivalence equation $E = mc^2$, where the mass of the earth is 6×10^{24} kg.

18. Use the diffusion theory to estimate light penetration in biological tissues. A 10 mW isotropic point source is buried in an infinite turbid medium. Assume that the absorption coefficient is 0.1 cm^{-1}, the scattering coefficient of a 5-cm-thick tissue is 100 cm^{-1}, the scattering anisotropy is 0.9, and the wavelength of light is 0.5 μm. Calculate the light fluence rate 5 cm from the source.

19. Use diffusion theory to estimate sonoluminescence light transmission in biological tissues. A 1 mW isotropic point source is buried in an infinite turbid medium. Assume that the absorption coefficient is 0.1 cm^{-1}, the scattering coefficient is 100 cm^{-1}, and the scattering anisotropy is 0.9. Calculate the light fluence rate integrated over a sphere of a 5 cm radius centered at the source.

20. What additional information does the phase measurement in a frequency-domain imaging technique provide compared with the continuous wave technique that measures only the amplitude of the diffuse light?

Suggested Readings

G. Boisdé, A. Harmer, Chemical and Biochemical Sensing with Optical Fibers and Waveguides, Artech House, Boston and London, 1996.

M. Born, E. Wolf, Principles of Optics, seventh expanded ed., Cambridge University Press, 1999.

B. Culshaw, J. Dakin, Optical Fiber Sensors: Vols. I and II, Artech House, Boston and London, 1989.

F.A. Duck, Physical Properties of Tissue, Academic, London, 1990.

E. Hecht, Optics, Addison-Wesley, Reading, MA, 1987.

A. Katzir, Lasers and Optical Fibers in Medicine, Academic Press Inc., San Diego, CA, 1993.

J. Lakowicz, Principles of Fluorescence Spectroscopy, second ed., Kluwer Academic/Plenum Publishers, 1999.

F.L. Pedrotti, L.S. Pedrotti, Introduction to Optics, second ed., Prentice Hall, Upper Saddle River, NJ, 1993.

V. Tuchin, Tissue Optics: Light Scattering Methods and Instruments for Medical Diagnosis, Society of Photo-Optical Instrumentation Engineers Press, Bellingham, Washington, 2000.

T. Vo-Dinh, Biomedical Photonics Handbook, CRC Press, January 24, 2003.
L.V. Wang, H.-I. Wu, Biomedical Optics: Principles and Imaging, Wiley, 2007.
A.J. Welch, M.J.C. van Gemert, Optical-Thermal Response of Laser Irradiated Tissue, Plenum Press, New York and London, 1995.
H.H. Willard, L.L. Merritt., J.A. Dean, F.A. Settle, Instrumental Methods of Analysis, seventh ed., Wadsworth Publishing Inc., Belmont, CA, 1988.